Strengthening Medial Olivocochlear Feedback Reduces the Developmental Impact of Early Noise Exposure

Authors: Valeria C. Castagna[1,2,3], Luis E. Boero[1,2,3], Mariano N. Di Guilmi[1], Camila Catalano Di Meo[1,2,3], Jimena A. Ballestero[2], Paul A. Fuchs[4,5], Amanda M. Lauer[4,5,6], Ana Belén Elgoyhen[1,2] and Maria Eugenia Gomez-Casati[2]

Running Title: Early Noise Protection via MOC Feedback

Affiliations:

[1]Instituto de Investigaciones en Ingeniería Genética y Biología Molecular, Dr. Héctor N. Torres, Consejo Nacional de Investigaciones Científicas y Técnicas, 1428 Buenos Aires, Argentina.

[2]Instituto de Farmacología, Facultad de Medicina, Universidad de Buenos Aires, 1121 Buenos Aires, Argentina and Consejo Nacional de Investigaciones Científicas y Técnicas, Argentina.

[3]Universidad de Buenos Aires, Facultad de Ciencias Exactas y Naturales, Departamento de Fisiología y Biología Molecular y Celular, 1428 Buenos Aires, Argentina.

[4]Department of Otolaryngology-Head and Neck Surgery, Johns Hopkins University School of Medicine; Baltimore, Maryland 21205, United States.

[5]Department of Neuroscience, Johns Hopkins University School of Medicine, Baltimore, Maryland 21205, United States.

[6]Center for Functional Anatomy and Evolution, Johns Hopkins University, School of Medicine, Baltimore, Maryland 21205, United States.

Corresponding Author: María Eugenia Gómez-Casati, Ph.D.
Instituto de Farmacología. Facultad de Medicina. Universidad de

Buenos Aires.

Address: Paraguay 2155. C1121ABG, Buenos Aires, Argentina.

Phone: 54-11-52853350

E-mail: mgomezcasati@fmed.uba.ar, megomezcasati@gmail.com

Number of Pages: 41

Number of Figures: 8

Number of words Abstract: 250

Number of words Introduction: 660

Number of words Discussion: 1497

Conflict of Interest: The authors declare no competing financial or non-financial interest.

Acknowledgements: This research was supported by Agencia Nacional de Promoción Científica y Técnica (Argentina) to M.E.G-C and NIH Grant R01 DC001508 (P.A.F, A.M.L, A.B.E and M.E.G-C) and the David M. Rubenstein Fund for Hearing Research.

Author Contributions: V.C.C, L.E.B, M.N.D-G, P.A.F, A.M.L, A.B.E and M.E.G-C designed research; V.C.C, C. C.dM and J.A.B performed experiments; V.C.C analyzed data. M.E.G-C wrote the paper. All authors discussed the results, read, edited, and commented on the manuscript.

Abstract

The early onset of peripheral deafness significantly alters the proper development of the auditory system. Likewise, exposure to loud noise during early development produces a similar disruptive effect. Before hearing onset in altricial mammals, cochlear inner hair cells exhibit spontaneous electrical activity that drives auditory circuit development. This activity is modulated by medial olivocochlear (MOC) efferent feedback through α9α10 nicotinic cholinergic receptors in inner hair cells. In adults, these receptors are restricted to outer hair cells, where they mediate MOC feedback to regulate cochlear amplification. Although the MOC system's protective role to prevent noise-induced hearing loss in adulthood is well-established, its influence during early developmental stages -especially in response to exposure to loud noise- remains largely unexplored. In this study, we investigated the role of MOC feedback during early postnatal development using α9 knockout (KO) and α9 knock-in (KI) mice of either sex, which respectively lack or exhibit enhanced cholinergic activity. Our findings reveal that both increased and absent olivocochlear activity result in altered auditory sensitivity at the onset of hearing, along with long–range alterations in the number and morphology of ribbon synapses. Early noise exposure caused lasting auditory damage in both wild-type and α9KO mice, with deficits persisting into adulthood. In contrast, α9KI mice were protected from noise-induced damage, with no long-term effects on auditory function. These results highlight the increased susceptibility of the auditory system during early postnatal development. Moreover, they indicate that an enhanced MOC feedback shields the auditory system from noise damage during this period.

SIGNIFICANCE STATEMENT

Early development represents a sensitive window for shaping auditory function. We show that the medial olivocochlear system is critical for establishing normal ribbon synapse density and size; key features for proper hearing onset. We also show that the developing auditory system is

73 especially vulnerable to loud noise, with early exposure causing more severe and lasting effects
74 than similar noise later in life. Notably, enhancing α9α10 nAChR receptor activity during this early
75 stage offers protection against noise-induced damage, revealing a time-sensitive opportunity to
76 safeguard auditory development.
77

Introduction

Cochlear and central auditory system development relies on tightly coordinated cellular and molecular events, with critical refinements during early postnatal life to optimize sound encoding (Sanes and Walsh, 1998). Noise exposure during this sensitive period can disrupt these mechanisms, damaging cochlear structures and neural circuits (Chang and Merzenich, 2003; Keuroghlian and Knudsen, 2007; Zhou and Merzenich, 2008; Sanes and Bao, 2009; Lauer et al., 2011). Early acoustic exposure affects neuronal sensitivity, innervation, frequency tuning and response characteristics across the auditory pathway (Caminos et al., 2005; Waguespack et al., 2007; Sanes and Bao, 2009; Dorrn et al., 2010; Sun et al., 2010; Froemke and Jones, 2011). Such disruptions can lead to permanent auditory deficits, emphasizing the importance of safeguarding the developing auditory system.

In altricial mammals, inner hair cells (IHCs) exhibit spontaneous electrical activity that propagates into the central nervous system (CNS) before hearing onset (~P12 in mice) (Lippe, 1994; Marcotti et al., 2003; Sonntag et al., 2009; Tritsch and Bergles, 2010; Johnson et al., 2011; De Faveri et al., 2025). This activity is crucial for neuronal survival and for refining auditory circuits (Tierney et al., 1997; Friauf and Lohmann, 1999; Mostafapour et al., 2000; Leake et al., 2006; Clause et al., 2014; Di Guilmi et al., 2019). During this period, MOC neurons from the superior olivary complex form transient axosomatic synapses with immature IHCs, modulating their spontaneous firing (Glowatzki and Fuchs, 2000; Marcotti et al., 2004; Johnson et al., 2013). These synapses, mediated by α9α10 nicotinic cholinergic receptors (nAChRs) coupled to SK2 channels, hyperpolarize IHCs (Glowatzki and Fuchs, 2000; Marcotti et al., 2004; Goutman et al., 2005), shaping burst patterns that guide synaptic development and ensure bilateral representation in the CNS (Walsh et al., 1998; Johnson et al., 2013; Clause et al., 2014; Di Guilmi et al., 2019; Wang et al., 2021). As IHCs mature, they lose direct efferent contacts and no longer respond to acetylcholine (ACh) (Katz et al., 2004; Roux et al., 2011). At this stage, MOC fibers cross the

103 tunnel of Corti and innervate OHCs to regulate cochlear amplification (Wheeler et al., 1994;
104 Ernfors et al., 1995; Knipper et al., 1995; Simmons et al., 1996; Walsh et al., 1998; Vattino et al.,
105 2020). ACh-induced responses in OHCs emerge by P6, shifting from nicotinic-like to outward
106 potassium currents by hearing onset (Dulon and Lenoir, 1996; He and Dallos, 1999). The
107 olivocochlear system matures rapidly within the first 2–3 postnatal weeks, with adult-like
108 innervation by the end of the first month (Pujol et al., 1978; Pujol, 1985; Simmons et al., 1990,
109 1996). While the protective role of the MOC system in preventing noise-induced hearing loss in
110 adulthood is well-documented (Liberman, 1991; Maison and Liberman, 2000; Maison et al., 2002,
111 2013; Taranda et al., 2009; Boero et al., 2018), its impact during early developmental stages,
112 remains largely unexplored.

113 This study explores how cholinergic MOC input strength influences auditory development
114 and noise vulnerability during this sensitive period. We used mice with altered α9α10 nAChR
115 activity: α9KO mice, which lacks efferent transmission (Vetter et al., 1999), and α9KI, carrying an
116 α9 point mutation that leads to an enhanced MOC effect (Taranda et al., 2009). We show that
117 MOC strength modulates hearing onset timing and IHC ribbon synapse formation. Wild-type (WT)
118 mice exposed to noise at hearing onset showed greater threshold shifts and synaptic loss than
119 similar exposure in adulthood (Boero et al., 2018), revealing heightened developmental
120 vulnerability. In α9KO mice, early exposure resulted in a persistent loss of auditory nerve
121 synapses, emphasizing the essential role of the MOC pathway. Conversely, α9KI mice were
122 protected from both thresholds shifts and synaptic loss after early noise exposure. This protection
123 occurred during a developmental window when the auditory system is still maturing and MOC-
124 OHC synapses are forming (Simmons et al., 1996; Vattino et al., 2020). These findings highlight
125 the importance of efferent cholinergic input during cochlear development and suggest that
126 strengthening MOC feedback during this window can mitigate long-term effects of early acoustic
127 trauma.

128

129 **Materials and Methods**

130 **Animals.** α9KO and α9KI mice have been previously described (Vetter et al., 1999; Taranda et
131 al., 2009) and were backcrossed with the congenic FVB.129P2-*Pde6bþ Tyrc-ch/AntJ* strain
132 (https://www.jax.org/strain/004828) for seventeen generations (i.e., N-17). We maintained a
133 consistent male-to-female ratio across all experimental groups and genotypes. No sex-related
134 differences were observed in the data. This study included adult and pup animals aged P12 to
135 P75, which were housed in a sound-controlled room within the animal care facility. Background
136 sound levels in this environment were consistently below 50 dB SPL. Noise levels were measured
137 using an electret condenser microphone (FG-23329-PO7; Knowles). Transient sounds during
138 routine cage cleaning and daily maintenance by animal care staff were minimal, with peaks not
139 exceeding 70 dB SPL. The methods reported in this study adhere to the ARRIVE guidelines for
140 reporting *in vivo* animal research (https://arriveguidelines.org/), ensuring transparency and
141 reproducibility. All procedures were conducted in accordance with institutional and ethical
142 guidelines for animal care and use.

143

144 **Auditory function tests.** Physiological assessments of cochlear and central function, including
145 auditory brainstem responses (ABRs) and distortion-product otoacoustic emissions (DPOAEs),
146 were performed in mice anesthetized with xylazine (10 mg/kg, i.p.) and ketamine (100 mg/kg, i.p.)
147 and placed in a soundproof chamber maintained at 32°C to counteract the drop in body
148 temperature caused by anesthesia. ABR represents sound-evoked potentials generated by
149 neural circuits in the ascending auditory pathways, while DPOAEs are sounds emitted by the
150 cochlea, specifically by OHCs, in response to two pure-tone stimuli presented simultaneously.
151 Sound stimuli were delivered through a custom acoustic system with two dynamic earphones
152 used as sound sources (CDMG15008–03A; CUI) and an electret condenser microphone (FG-

153 23329-PO7; Knowles) coupled to a probe tube to measure sound pressure near the eardrum.
154 Data collection was conducted using a National Instruments PXI-based system equipped with 24-
155 bit input/output boards and operated through a custom LabView software interface. For ABRs,
156 platinum needle electrodes were placed into the skin at the dorsal midline close to the neural crest
157 and pinna with a ground electrode near the tail. ABR potentials were evoked with 5 ms tone pips
158 (0.5 ms rise-fall, with a $\cos^2$ envelope, at 40/s) delivered to the eardrum at log-spaced frequencies
159 from 5.6 to 45.25 kHz. The response was amplified 10,000X with a 0.3–3 kHz passband. Sound
160 level was raised in 5 dB steps from 20 to 80 dB sound pressure level (SPL). At each level, 1024
161 responses were averaged with alternated stimulus polarity. Threshold for ABR was defined as
162 the lowest stimulus level (<80 dB SPL) at which a repeatable wave 1 could be identified in the
163 response waveform. The ABR wave 1 amplitude was computed by off-line analysis of the peak-
164 to-peak amplitude of stored waveforms. The DPOAEs in response to two primary tones of
165 frequency f1 and f2 were recorded at 2f1-f2, with f2/f1=1.2, and the f2 level 10 dB lower than the
166 f1 level. Ear-canal sound pressure was amplified and digitally sampled at 4 μs intervals. DPOAE
167 threshold was defined as the lowest f2 level in which the signal to noise floor ratio is >1.
168
169 **Noise exposure.** Animals were exposed under anesthesia at P15 to broadband noise (1–16 kHz,
170 100 dB SPL) for 1 hour using closed-field earphones (CDMG15008–03A; CUI) as the sound
171 source. This broader frequency range was selected to induce significant threshold shifts in the
172 apical region of the cochlea, as previously described in (Boero et al., 2018). Noise exposure was
173 conducted in the same acoustic chamber used for cochlear function tests. The noise consisted of
174 a flat-spectrum broadband signal calibrated to the target SPL immediately before each exposure
175 session.
176
177 **Animal monitoring and health assessment.** To assess the impact of repeated anesthesia on

178 the health and well-being of the animals, their weight and motor activity were monitored daily
179 throughout the auditory function recordings and noise exposure protocols. Animals were observed
180 during their recovery from anesthesia to ensure no adverse effects on their general condition.
181 Growth curves showed no significant differences in weight between animals that were
182 anesthetized and untreated controls animals, suggesting that anesthesia did not affect normal
183 growth. Furthermore, no behavioral changes or motor impairments were observed in the
184 anesthetized animals when compared to controls, indicating that repeated anesthesia had no
185 detectable impact on overall health or behavior.
186
187 **Cochlear processing and immunostaining.** Cochleae were perfused intralabyrinthly with 4%
188 paraformaldehyde (PFA) in phosphate-buffered saline (PBS), post-fixed with 4% PFA overnight,
189 and decalcified in 0.12 M EDTA. Cochlear tissues were microdissected and permeabilized by
190 freeze/thaw cycles in 30% sucrose. The dissected samples were then separated into distinct wells
191 based on cochlear region: apex, middle and base. Tissue samples were blocked with 5% normal
192 goat serum and 1% Triton X-100 in PBS for 1 h, followed by incubation in primary antibodies
193 (diluted in blocking buffer) at 37°C for 16 h. The primary antibodies used in this study were: 1)
194 anti-C-terminal binding protein 2 (mouse anti-CtBP2 IgG1; BD Biosciences, San Jose, CA;
195 Cat#612044, RRID:AB_399431, 1:200) to label the presynaptic ribbon, 2) anti-glutamate receptor
196 2 (mouse anti-GluA2 IgG2a; Millipore, Billerica, MA; Cat#MAB397, RRID:AB_11212990, 1:2000)
197 to label the post-synaptic receptor plaques and 3) anti-Myosin 7a (rabbit anti-MyosinVIIa, Proteus
198 Biosciences; Cat# 25-6790, RRID:AB_10015251, 1:200) to label the cochlear hair cells. Tissues
199 were then incubated with the appropriate Alexa Fluor-conjugated fluorescent secondary
200 antibodies (Invitrogen, Carlsbad, CA; 1:500 in blocking buffer) for 2 hours at room temperature.
201 Finally, tissues were mounted on microscope slides in FluorSave mounting media (Millipore,
202 Billerica, MA).

Confocal microscopy and image processing. For IHC synaptic counts, cochlear tissue from the apex, middle and base regions was first imaged at low magnification to correlate each piece with its corresponding frequency region (Müller et al., 2005). The apical region corresponds to 4–12 kHz, the middle region to 12–20 kHz, and the base region to 22–40 kHz. Z-stacks images were then acquired using a Leica TCS SPE microscope with a 63X oil-immersion lens (1.5X or 4X digital zoom). Imaging settings were consistent across all samples, ensuring no pixel saturation. For each stack, the Z-step was set to 0.3 µm, with a pixel size of 0.11 µm in both the X and Y axes. Each stack typically contained 10 to 20 IHCs. Image stacks were processed using Fiji software (RRID:SCR_002285) (Schindelin et al., 2012), and a custom plugin was developed to automate the counting of synaptic ribbons, glutamate receptor patches and co-localized synaptic puncta. The algorithm's accuracy was validated by comparing automated counts to manual counts, ensuring reliable quantification. Briefly, each channel was analyzed separately, and maximum projections were generated to quantify the number of CtBP2 or GluA2 puncta. Additionally, a composite between the three channels was produced to draw the different regions of interest (ROI) that correspond to each IHC taking the myosin staining as a reference. The maximum projections from the single channels were multiplied to generate a merged 32-bit image. Then, they were converted to binary images after a custom thresholding procedure. An automatic counting of the number of particles on each ROI was performed. The plugin used for synapse quantification, along with detailed instructions, is available at: https://github.com/vcastagna/CountsSynapses.

For quantitative volumetric synaptic analysis, different regions from the whole cochlea were imaged and confocal z-stacks were processed in Fiji. z-stacks were deconvolved applying 10 iterations of the Richardson-Lucy algorithm in the DeconvolutionLab2 plugin (Sage et al., 2017), an algorithm that has been used previously in cochlear whole mounts (Jing et al., 2013).

228 Then, the 3D Object Counter plugin was used to perform three-dimensional image segmentation
229 and object individualization of the deconvoluted stacks. According to previous work (Liberman et
230 al., 2011; Gilels et al., 2013; Paquette et al., 2016) we reasoned that a synapse would occupy a
231 volume between 0.04 μm3 to 5 μm3, and then we set a size range of 20-2000 voxels, with a voxel
232 size of 0.11 μm x 0.11 μm x 0.2 μm. The volumes of presynaptic ribbons (CtBP2 fluorescence)
233 and postsynaptic AMPA receptor clusters (GluA2 fluorescence) at IHC-afferent synapses were
234 measured using the 3D ROI Manager (Ollion et al., 2013). All exported volumes were checked to
235 ensure that volumes were within instrument resolution limits after threshold adjustments.
236
237 **Statistical analysis.** Data was analyzed using R Statistical Software (RRID:SCR_001905).
238 Shapiro-Wilks test was used for testing normal distribution of the residuals. In cases where the
239 data did not follow a normal distribution, the following tests were used: Kruskal-Wallis test followed
240 by multiple contrasts according to Dunn's method for comparisons between three groups (IHCs
241 synaptic counts in the control condition, ABR and DPOAE thresholds during development) and
242 Mann-Whitney U test for comparisons between two groups (ABR thresholds, DPOAE thresholds,
243 and IHCs synaptic counts). If data were normally distributed, a one-way ANOVA was conducted,
244 followed by Holm-Sidak post hoc tests for three-group comparisons (wave 1 amplitudes and
245 synaptic volumes in the control condition). For two-group comparisons, a t-test was used (synaptic
246 volumes). Statistical significance was set to $p<0.05$.
247
248 **Results**
249 **Onset of auditory perception in mice with varying levels of efferent inhibition**
250 In this study we used mice with distinct levels of α9α10 nAChR activity: 1) WT, with normal
251 MOC function; 2) α9KO, which lacks cholinergic transmission between MOC neurons and hair
252 cells (Vetter et al., 1999), and 3) α9KI mice carrying an α9 nAChR subunit point mutation that

253 leads to enhanced responses to ACh (Taranda et al., 2009). To explore the impact of noise
254 exposure at hearing onset, we first identified the optimal developmental stage for introducing such
255 exposure, by assessing the onset of hearing under control (unexposed) conditions in these mouse
256 models. This was done by tracking auditory brainstem responses (ABRs), the sound-evoked
257 potentials generated by neuronal circuits in the ascending auditory pathway, at different postnatal
258 ages across the three groups. Individual ABR waves reflect the activation of auditory periphery
259 and brainstem processing relay stations within the first ~7 ms after sound stimulus onset
260 (Buchwald and Huang, 1975; Karplus et al., 1988; Shapiro, 1988; Shaw, 1988; Melcher and
261 Kiang, 1996; Kim et al., 2013). Wave 1 represents the synchrony in firing of spiral ganglion
262 neurons and is highly correlated with the number of synapses between IHCs and auditory nerve
263 fibers (Buchwald and Huang, 1975; Antoli-Candela and Kiang, 1978; Kujawa and Liberman,
264 2009). Measurements were taken daily from P12 to P16, as well as P22 and P75, in anesthetized
265 mice. Interestingly, we found that ABR onset occurred earlier in α9KI mice, with enhanced MOC
266 function, compared to WT mice with normal MOC synapses and was delayed in α9KO mice
267 lacking α9α10 nAChR activity (Figure 1a and b). Representative ABR traces recorded at P14 in
268 response to a 16 kHz stimulus across varying intensities illustrate differences in ABR thresholds
269 among the three mouse groups with distinct levels of α9α10 nAChR activity (Figure 1a). At this
270 developmental stage, α9KI mice exhibited lower ABR thresholds, and more distinct peaks at
271 suprathreshold intensities compared to WT mice. In contrast, α9KO mice showed higher ABR
272 thresholds relative to WT mice (Figure 1a). Figure 1b shows the mean ABR thresholds measured
273 at test frequencies of 11.33, 16, and 22.65 kHz from P12 to P75 across the three groups of mice.
274 A comparison between α9KI and WT mice revealed that α9KI mice displayed measurable ABR
275 responses as early as P13 (Kruskal-Wallis, followed by Dunn's test, degree of freedom [df] = 2, p
276 = 0.01 at 22.65 kHz; Figure 1b) and achieved mature threshold levels earlier than their WT
277 littermates (Kruskal-Wallis, followed by Dunn's test, df = 2, p = 0.02 at 16 and 22.65 kHz at P14;

Figure 1b). In contrast, ABR onset was delayed by a day in α9KO compared to WT mice (Kruskal-Wallis followed by Dunn's test, df = 2, p = 0.04 at 11.33 and 16 kHz; Figure 1b), indicating that cochlear maturation is slower in the absence of pre-hearing efferent modulation. To summarize, at P13, no ABR responses were observed in WT (0 out of 9) or α9KO (0 out of 7) mice in response to tone pips at 80 dB SPL across 11.33, 16, and 22.65 kHz. In contrast, 6 out of 9 α9KI mice exhibited ABR responses at P13. By P14, ABR responses were present in 77.7% of WT mice at 11.33 and 22.65 kHz and in 100% at 16 kHz. Meanwhile, 85% of α9KO mice responded at all frequencies, but with higher thresholds than WT (Figure 1b). All α9KI mice exhibited robust responses at all tested frequencies by P14. By P15, 100% of WT and 91% of α9KO mice showed ABR responses.

Tone pip-evoked ABR wave 1 amplitudes were then analyzed at a suprathreshold level of 80 dB SPL at the different test frequencies in the three groups of mice with varying levels of α9α10 nAChR activity (Figure 2a, b). As illustrated in the representative traces in Figure 2a, measurable ABR wave 1 amplitudes at P13 were only observed in α9KI mice. At P14, the number of discernible peaks were fewer in WT and α9KO mice compared to α9KI mice. Up to P15, response peaks at 80 dB SPL were slightly larger and more distinct in α9KI mice, reflecting enhanced auditory responses during this postnatal developmental window. However, starting at P16, α9KI mice exhibited smaller ABR wave 1 amplitudes, with significant differences observed at P75 at 16 and 22.65 kHz compared to WT mice (one way ANOVA followed by Holm-Sidak test, df = 2, p = 0.03 at both frequencies; Figure 2b). In α9KO mice, wave 1 amplitudes remained smaller than those of WT and α9KI mice until P16, with the difference being significant at 22.65 kHz (one way ANOVA followed by Holm-Sidak test, df = 2, p = 0.02; Figure 2b). These findings align with the ABR threshold results, indicating that the strength of efferent cholinergic inhibition to hair cells contributes to the timely development of auditory function. The reduced ABR wave 1 amplitudes obtained in mature mice with either enhanced or null cholinergic activity indicates that proper

303 MOC modulation during development might be crucial for the correct formation of auditory nerve
304 synapses. Analysis of ABR wave 1 latencies at different postnatal ages showed no significant
305 differences between genotypes (Figure 2c). While wave 1 latencies were consistently longer
306 across all groups at P14, they shortened to levels typical of mature mice by P15.

307 OHC function was assessed through distortion-product otoacoustic emissions (DPOAE)
308 at the different postnatal ages. In a healthy cochlea, two close pure tones produce distortions due
309 to OHC nonlinearities, which are amplified by OHC electromotility and detected with a microphone
310 in the external ear canal (Shera and Guinan Jr., 1999; Robles and Ruggero, 2001). DPOAE
311 responses followed a similar pattern to ABR thresholds, though the differences were not
312 statistically significant (Kruskal-Wallis, df = 2, $p > 0.05$ at all frequencies; Figure 1c). At P13,
313 DPOAE responses were nearly absent in WT (1 out of 9) and α9KO (0 out of 7) mice across the
314 tested frequencies. In contrast, 3 out of 9 α9KI mice showed DPOAE responses at 16 and 22.65
315 kHz. By P14, DPOAE responses were detectable in 75% of WT and α9KO mice at 16 and 22.65
316 kHz, and in 60% of mice at 11.33 kHz. All α9KI mice exhibited strong DPOAE responses at all
317 tested frequencies by P14. By P15, response rates reached 100% in both WT and α9KO mice.
318 Note that at P22 and P75, mean ABR and DPOAE thresholds in α9KI mice were slightly elevated
319 by 5–10 dB compared to WT and α9KO mice (Figure 1b, c). This elevation reached statistical
320 significance only for ABR thresholds at P22 (Kruskal-Wallis, df = 2, $p = 0.03$ at 11.33 kHz; $p =$
321 0.04 at 16 kHz and $p = 0.02$ at 22.65 kHz). The elevated thresholds in α9KI mice at these mature
322 stages are most likely due to enhanced suppression of OHCs activity resulting from increased
323 cholinergic neurotransmission. This effect, previously described by Taranda et al. (2009), can be
324 reversed by strychnine, a known antagonist of the α9α10 nAChR. Collectively, these findings
325 indicate that the onset of hearing is altered in mice with either absent or enhanced olivocochlear
326 cholinergic feedback.
327

ABR thresholds after noise exposure at hearing onset in mice with different degree of MOC inhibition

To investigate the impact of noise exposure during early development, we exposed WT, α9KO, and α9KI mice to loud noise at P15. This allowed us to evaluate how acoustic experience influences auditory function before full threshold maturation in each genotype. Mice were exposed to 1–16 kHz noise at 100 dB SPL for 1 hour at P15. Auditory responses were then assessed at 1-, 7-, and 60-days post-exposure to track functional changes over time.

Previous studies in WT mice exposed to the same noise protocol at P21 showed a significant increase in auditory thresholds of 10–35 dB SPL one day after exposure, which returned to baseline within a week, indicating a transient threshold shift (Boero et al., 2018). In contrast, as shown in Figure 3a, no changes in ABR thresholds were observed at P16, one day after noise exposure, across frequencies of 8, 16, and 22.65 kHz in WT mice compared to unexposed controls. Remarkably, ABR thresholds at P16 were slightly lower than those measured at P15, prior to noise exposure, and showed no significant difference when compared to unexposed controls at the same age. This suggests that noise did not have an immediate effect on the maturation of auditory thresholds at this postnatal developmental stage. One week after exposure, however, ABR thresholds were elevated at all frequencies in noise-exposed WT animals, and this increase persisted at the same level for at least two months post-exposure (Mann- Whitney test, df = 1, P22: $p = 0.006$ at 8 kHz; $p = 0.007$ at 16 kHz; $p = 0.002$ at 22.65 kHz and P75: $p = 0.04$ at 8 kHz; $p = 0.03$ at 16 kHz and $p = 0.04$ at 22.65 kHz; Figure 3a). This outcome contrasts with the transient threshold elevation observed in WT mice from the same genetic background, exposed at P21 using the same noise protocol (Boero et al., 2018), suggesting that noise exposure at this early developmental stage may disrupt the normal maturation process, potentially leading to more profound and lasting auditory deficits.

A similar trend as seen in WT mice was observed after exposing α9KO mice to noise at

353 P15 (Figure 3b). One day after exposure, there were no changes in ABR thresholds at 8, 16 and
354 22.65 kHz. However, seven days post-exposure, there was an elevation in auditory thresholds
355 across all frequencies (Mann-Whitney test, df = 1, p = 0.03 at 8 kHz; p = 0.01 at 16 kHz and p =
356 0.02 at 22.65 kHz), which, unlike in WT mice, returned to normal levels after two months (Mann-
357 Whitney test, df = 1, p > 0.05 at all frequencies; Figure 3b). Notably, in α9KI mice, ABR thresholds
358 were not affected by noise exposure at all the frequencies tested (Figure 3c), suggesting that at
359 this early age, the enhancement of cholinergic activity on OHCs provides protection from noise-
360 induced cochlear threshold elevations (Mann-Whitney test, df = 1, p > 0.05 at all frequencies).
361

362 **Amplitudes of cochlear sound-evoked potentials after noise exposure at hearing onset in**
363 **mice with different degree of efferent inhibition**

364 To assess the neural activity across auditory nerve fibers, we measured ABR wave 1
365 amplitudes at frequencies of 8, 16, and 22.65 kHz at different ages after noise exposure in the
366 three mouse groups (Figure 4). One day after noise exposure, we observed a reduction in wave
367 1 amplitudes across all frequencies in WT mice. Further testing of WT mice one week and two
368 months post-exposure revealed a significant and long-lasting reduction, indicating a permanent
369 decrease of ABR wave 1 amplitude (Mann- Whitney test, df = 1, P22: p = 0.007 at 8 kHz; p =
370 0.005 at 16 kHz; p = 0.005 at 22.65 kHz and P75: p = 0.04 at 8 kHz; p = 0.002 at 16 kHz and p =
371 0.002 at 22.65 kHz; Figure 4a). Similar permanent reductions in wave 1 amplitude were observed
372 in α9KO mice after exposure to noise at 16 and 22.65 kHz (Mann-Whitney test, df = 1, P22: p =
373 0.04 at 16 kHz; p = 0.001 at 22.65 kHz and P75: p = 0.03 at 16 kHz and p = 0.04 at 22.65 kHz;
374 Figure 4b). Notably, no changes in ABR wave 1 amplitudes were observed at any age post-
375 exposure in mice with enhanced α9α10 nAChR activity, suggesting a preservation of cochlear
376 synapses after noise exposure (Mann-Whitney test, df = 1, p > 0.05 at all frequencies; Figure 4c).
377

DPOAE thresholds after noise exposure at hearing onset in mice with different levels of α9α10 nAChR activity

To assess the impact of hearing onset noise exposure on the function of OHCs, we recorded DPOAEs at 8, 16, and 22.65 kHz on the three groups of mice with varying levels of MOC function (Figure 5). During early development, the auditory system undergoes significant maturation, reflected by a progressive decrease in DPOAE thresholds with age, as shown in Figure 1c. In WT mice, one day after noise exposure at P16, there was no difference in DPOAE thresholds between the noise-exposed group and unexposed controls (Figure 5a). However, when comparing DPOAE thresholds at P16 to those at P15 within both groups (i.e. exposed and unexposed controls), a clear reduction was observed (Figure 5a). This decline in thresholds underscores the natural maturation process of the auditory system, indicating that early noise exposure does not immediately disrupt the ongoing development of DPOAE thresholds at this early postnatal stage. By P22, seven days after noise exposure, an increase in DPOAE thresholds was observed that was statistically significant only at 16 kHz (Mann-Whitney, df = 1, $p = 0.01$; Figure 5a). Yet, two months later, DPOAE thresholds were comparable to those of unexposed WT controls across all tested frequencies, suggesting that early noise exposure did not result in long-term changes in OHC function (Figure 5a).

In α9KO mice, DPOAE thresholds remained unchanged one day after noise exposure. However, seven days post-exposure, significant threshold elevations were observed at 8 and 16 kHz, but not at 22.65 kHz (Mann-Whitney, df = 1, $p = 0.02$ at 8 kHz and $p = 0.02$ at 16 kHz). After two months, recovery to unexposed levels occurred only at 8 kHz, while DPOAE thresholds remained elevated at 16 kHz (Mann-Whitney, df = 1, $p = 0.003$ at 16 kHz; Figure 5b). In contrast, mice with enhanced MOC function showed no changes in DPOAE thresholds at any post-exposure time point (Figure 5c), suggesting that noise exposure at hearing onset did not impair the cochlear amplifier function in these mice with enhanced OHC inhibition.

403

404 **Ribbon synapse changes after early noise exposure in mice with different levels of α9α10**
405 **nAChR activity**

406 Histological analysis was performed on cochleae dissected and fixed at P15 and P75 from
407 unexposed mice of all three genotypes, which exhibit varying levels of α9α10 nAChR activity, to
408 evaluate its effect of on the density and structure of IHC ribbon synapses. To visualize these
409 ribbon synapses, we performed immunostaining on whole-mount preparations of the organ of
410 Corti with antibodies against CtBP2-Ribeye, a presynaptic ribbon protein (Khimich et al., 2005),
411 and GluA2, an AMPA-type glutamate receptor expressed at the postsynaptic afferent terminal
412 (Matsubara et al., 1996; Liberman et al., 2011; Maison et al., 2013). Ribbon synapses were
413 identified by the colocalization of CtBP2 and GluA2 puncta at the base of the IHC, as shown in
414 representative confocal images of IHC synapses from apical whole mount organ of Corti from
415 unexposed WT, α9KO, and α9KI mice (Figure 6a) (Liberman et al., 2011). We quantified the
416 number of colocalized synaptic markers per IHC at both ages across three cochlear regions, each
417 representing a distinct frequency range: apex (~4–12 kHz), middle turn (~12–20 kHz), and base
418 (~22–40 kHz) (Figure 6b). At the low-frequency apical end, both unexposed α9KO and α9KI mice
419 showed a significant reduction in synaptic density compared to WT, with decreases of 33% and
420 31.18% at P15, and 30.64% and 27.94% at P75, respectively (Kruskal-Wallis, df = 2, $p < 0.0001$
421 for both groups; Figure 6b, left panel). In the middle region, synaptic density was significantly
422 reduced in both α9KO and α9KI mice compared to WT at P15 (by 28.3% and 35.33%,
423 respectively). However, at P75, only α9KI mice showed a significant reduction (35.97%) relative
424 to WT (Kruskal-Wallis, df = 2, $p < 0.0001$; Figure 6b, middle panel). Similarly, in the high-frequency
425 basal region, synaptic puncta were significantly reduced at P15 in both α9KO and α9KI mice (by
426 24.9% and 24.3%, respectively; Kruskal-Wallis, df = 2, $p < 0.001$ in α9KO and $p < 0.01$ in α9KI;
427 Figure 6b, right panel), whereas at P75, a significant reduction of 22.07 % was observed only in

428 α9KI mice (Kruskal-Wallis, df = 2, p = 0.02; Figure 6b, right panel). No significant changes in the
429 number of synaptic puncta were observed between P15 and P75 in WT, α9KO, or α9KI mice
430 across any cochlear region (Figure 6b), indicating that under unexposed conditions, alterations in
431 transient MOC inhibition affect the number of ribbon synapses early in development and persist
432 into maturity.

433 We further quantified the volume of CtBP2 puncta and GluA2 receptor patches within
434 colocalized synaptic markers at both P15 and P75 across the three groups of mice (Figure 6c, d).
435 In the apical region, both α9KO and α9KI mice showed reduced ribbon volumes compared to WT
436 at both ages (one way ANOVA followed by Holm-Sidak test, df = 2, p < 0.0001, for both groups
437 and ages; Figure 6c, left panel). In the middle cochlear region at P15, CtBP2 puncta were
438 enlarged in α9KO mice and reduced in α9KI mice compared to WT. By P75, only α9KI mice
439 continued to show a significant reduction relative to WT (one way ANOVA followed by Holm-Sidak
440 test, df = 2, p < 0.0001, for both groups and ages; Figure 6c, middle panel). In the basal region,
441 CtBP2 volumes were increased in α9KO mice and reduced in α9KI mice at both ages (one way
442 ANOVA followed by Holm-Sidak test, df = 2, p < 0.0001, for both groups and ages; Figure 6c,
443 right panel). GluA2 receptor patch size was significantly reduced in the apical region of α9KI mice
444 compared to WT at both P15 and P75, while no changes were observed in α9KO mice (one way
445 ANOVA followed by Holm-Sidak test, df = 2, p < 0.0001, for both ages; Figure 6d, left panel). In
446 the middle region, no differences in GluA2 size were observed at P15; however, by P75, both
447 α9KO and α9KI mice exhibited reduced GluA2 volumes compared to WT. (one way ANOVA
448 followed by Holm-Sidak test, df = 2, p < 0.05 in α9KO and p < 0.0001 in α9KI; Figure 6d, middle
449 panel). In the basal region, GluA2 puncta were significantly larger in α9KO mice compared to WT
450 at both P15 and P75 (one-way ANOVA followed by Holm-Sidak test, df = 2, p < 0.01 at P15 and
451 p < 0.0001 at P75; Figure 6d, right panel), while no differences were observed in α9KI mice.
452 These results suggest that inhibitory input from cholinergic efferent fibers plays a key role in

453 shaping synaptic density and preserving the morphology of pre- and postsynaptic elements
454 essential for proper auditory function.

455 The long-term impact of noise exposure at hearing onset on auditory nerve synapse
456 numbers is illustrated in Figure 7, on cochleae dissected and fixed at P75 from control and noise-
457 exposed mice with varying levels of α9α10 nAChR activity. Presynaptic, postsynaptic, and
458 colocalized synaptic puncta quantifications are shown for the apical, middle, and basal cochlear
459 regions (Figure 7, violin plots, right panels). In WT exposed ears, the number of CtBP2, GluA2,
460 and colocalized synaptic puncta significantly decreased at both the apical and basal cochlear
461 ends (Figure 7a). The decrease in CtBP2 puncta was more pronounced in the high-frequency
462 basal region, with a 37.2% decrease compared to controls (Mann-Whitney, df = 1, $p < 0.0001$ at
463 the apical and basal regions). Similarly, GluA2 postsynaptic receptors were reduced in both the
464 apical and basal turns in the cochlea of noise-exposed WT mice (Mann-Whitney, df = 1, $p <$
465 0.0001 at both cochlear regions). Putative ribbon synapse counts, defined by juxtaposed CtBP2-
466 and GluA2-positive puncta, showed a 34.21% reduction in the apical and a 32.56% reduction in
467 the basal turn following acoustic trauma (Mann-Whitney, df = 1, $p < 0.0001$ at both cochlear
468 regions) (Figure 7a, right panel). In α9KO mice, there was also a reduction in the number of
469 presynaptic, postsynaptic, and colocalized puncta after noise exposure, depending on cochlear
470 frequency/location (Figure 7b). Ribbon puncta in α9KO exposed ears were reduced by up to
471 14.73% of the control in the apical and 24.75% in the basal cochlear ends after noise exposure
472 (Mann-Whitney, df = 1, $p = 0.001$ and $p = 0.002$ at the apical and basal region, respectively).
473 GluA2-positive postsynaptic receptor patches decreased by 24.79% in the basal turn of noise-
474 exposed mice (Mann-Whitney, df = 1, $p = 0.004$). Following noise exposure, synaptic puncta were
475 reduced by 26.17% in the apical cochlear region and 25.87% in the basal region (Mann-Whitney,
476 df = 1, $p = 0.002$ and $p < 0.0001$ at the apical and basal region, respectively) (Figure 7b, right
477 panel). Interestingly, after two months post-exposure, α9KI ears exhibited no significant changes

478 in presynaptic ribbons, postsynaptic GluA2 receptor patches, or putative synapses across all
479 cochlear regions (Figure 7c). Although not statistically significant, a modest increase in synaptic
480 density (~19% at the basal region) was observed in α9KI tissue (Figure 7c, right panel).

481 Finally, we quantified the volume of ribbons and AMPA receptor patches (i.e., colocalized
482 CtBP2 and GluA2 puncta) in unexposed and exposed mice with different levels of MOC feedback
483 (Figure 8). In WT mice, noise exposure resulted in significantly larger ribbon volumes in the basal
484 end of the cochlea compared to unexposed mice, with no corresponding changes in AMPA
485 receptor patch size (t-test, df = 1, p = 0.01; Figure 8a). No changes were observed in the apical
486 or middle cochlear regions (Figure 8a). Conversely, α9KO mice showed reduced volumes of both
487 ribbons and AMPA receptor patches in the basal region following noise exposure, with no
488 changes in the apical or middle regions (t-test, df = 1, p = 0.002 for CtbP2 volume and p = 0.003
489 for GluA2 volume; Figure 8b). Notably, α9KI mice showed no morphological changes, suggesting
490 that enhanced α9α10 nAChR activity protects synapses from noise-induced alterations (Figure
491 8c).

492

493 **Discussion**

494 Auditory development is a gradual process that begins during embryonic stages and
495 continues through sensitive postnatal periods. While the detrimental effects of noise exposure in
496 adulthood are well documented, less is understood about its impact during development and the
497 role of the MOC system in this context. Here, we show that varying levels of MOC inhibition impact
498 the timing of hearing onset and are crucial for proper development of IHC ribbon synapses. Early
499 noise exposure caused lasting auditory deficits in WT, highlighting the greater developmental
500 vulnerability. In contrast, enhanced cholinergic activity prevented damage, underscoring the
501 MOC's protective role in early development.

502 Before hearing begins, MOC synapses modulate IHCs' activity, shaping the

503 developmental increase in Ca^{2+} sensitivity of glutamate release at IHC ribbon synapses
504 (Glowatzki and Fuchs, 2000; Johnson et al., 2011, 2013). Disruption of this input, via genetic
505 modification or neonatal olivocochlear bundle transection, impairs cochlear and auditory circuit
506 maturation (Walsh et al., 1998; Frank et al., 2009; Hirtz et al., 2011; Johnson et al., 2013; Clause
507 et al., 2014; Di Guilmi et al., 2019; Babola et al., 2021). Our findings demonstrate that α9α10
508 nAChR activity regulates hearing onset and synaptic integrity. Enhanced α9α10 nAChR activity
509 in α9KI mice accelerates the onset of hearing, with sound-evoked potentials detected earlier than
510 in WT mice. In α9KO mice, which lack MOC input, hearing onset was delayed, with elevated ABR
511 thresholds and diminished wave 1 amplitudes. This aligns with prior reports using Ca^{2+} imaging
512 showing diminished sensitivity in α9KO inferior colliculus at hearing onset (Wang et al., 2021).
513 Importantly, both enhanced and absent MOC inhibition disrupted IHC ribbon synapse
514 development, with reduced synapse density and altered volumes at P15 and P75. Despite similar
515 synaptic reductions, their distinct ABR phenotypes suggest differential effects on auditory nerve
516 fiber subtypes. The earlier hearing onset in α9KI mice could reflect preservation or accelerated
517 maturation of low-threshold, high-spontaneous-rate fibers, while their disruption in α9KO mice
518 may contribute to delayed onset. Morphologically, α9KI mice showed reduced ribbon and GluA2
519 patch volumes across all cochlear turns, whereas α9KO mice exhibited region-specific changes:
520 smaller ribbons in apical regions with unchanged GluA2 patches, and enlarged pre- and post-
521 synaptic components in middle/basal turns. These ribbon alterations may reflect disruption of
522 Ca^{2+}-dependent ribbon fusion or stabilization, impairing synaptic refinement. Ribbon size and
523 maturation is tightly regulated by presynaptic Ca^{2+} influx (Frank et al., 2009; Sheets et al., 2012;
524 Wong et al., 2019; Özçete and Moser, 2021). Fusion of ribbon precursors during this period is
525 thought to support sustained release at mature active zones (Michanski et al., 2019). In
526 developing IHCs, intracellular Ca^{2+} dynamics are shaped by voltage-gated Ca^{2+} channels and by
527 α9α10 nAChRs, which are highly permeable to Ca^{2+} (Weisstaub et al., 2002; Gomez-Casati et

528 al., 2005; Moglie et al., 2018). In α9KO mice, the absence of α9α10-mediated Ca^{2+} influx leads to
529 increased action potential frequency and disrupted exocytosis (Johnson et al., 2013). In α9KI
530 mice, the L9'T mutation reduces receptor desensitization, likely prolonging Ca^{2+} entry and altering
531 IHC firing during the prehearing period (Taranda et al., 2009). These results highlight the MOC
532 synapse's role in coordinating afferent and efferent activity for normal auditory development.

533 Auditory sensitivity in vertebrates matures from high thresholds and poor tuning at hearing
534 onset to precise, low-threshold processing (Song et al., 2006). In WT mice, ABR and DPOAE
535 data from P12 to P75 showed this progression. At P14, thresholds were elevated and waveforms
536 immature, but by P22, thresholds and wave 1 amplitudes reached mature levels. Thus, at P15,
537 the time of noise exposure, auditory maturation was still incomplete. A key finding of this study is
538 that noise exposure during early development leads to more severe and lasting effects than those
539 reported at later stages. In WT mice, noise exposure at P15 caused lasting threshold shifts and
540 35% synapse loss, while the same exposure at P21 led to only transient threshold shifts and
541 milder synaptopathy (Boero et al., 2018). This underscores the heightened vulnerability at hearing
542 onset, likely due to both noise-induced damage and disruption of ongoing synaptic or hair cell
543 maturation. Similar age-dependent vulnerability has been reported in other juvenile models
544 (Fernandez et al., 2015; Jensen et al., 2015; Schrode et al., 2022; Lu et al., 2024). While the
545 mechanisms behind this heightened sensitivity remain unclear, it may arise from ongoing
546 maturation of the MOC system and central auditory pathways, including myelination and afferent
547 input. Developing interactions between the auditory nerve and LOC system may further increase
548 susceptibility to noise exposure.

549 In WT mice, DPOAE thresholds were elevated seven days post-exposure, reaching
550 statistical significance at 16 kHz, but returned to baseline by two months, suggesting preserved
551 or repaired OHC function. Whether this reflects true recovery, delayed maturation, or
552 compensation remains to be determined. In contrast, persistent ABR threshold elevation and

553 reduced wave 1 amplitudes suggest lasting afferent damage, likely due to cochlear synaptopathy
554 affecting both high- and low-threshold auditory nerve fibers (Reijntjes et al., 2025). This is the first
555 report of sustained ABR threshold elevation following moderate noise exposure, similar to lasting
556 high-frequency shifts and presynaptic loss seen in P14 rats and noise-sensitive P15 C57BL/6J
557 mice (Davis et al., 2003) exposed to high-intensity sound (Rybalko et al., 2015; Boero et al.,
558 2021). Noise exposure caused significant ribbon synapse loss in apical and basal cochlear
559 regions of WT mice, correlating with reduced ABR wave 1 amplitudes; however, despite functional
560 deficits at 16 kHz, synaptic loss in the mid-frequency region was minimal—reflecting a known
561 mismatch due to cochlear place-frequency map shifts after noise exposure (Müller and Smolders,
562 2005). In addition, IHCs of noise-exposed mice tend to have larger ribbons, especially in the basal
563 turn. Similar post-trauma ribbon enlargement was observed in RIBEYE-tagRFP mice (Mohamad
564 et al., 2024) and via volume EM (Lu et al., 2024), likely reflecting the fusion of individual ribbons.
565 Multi-ribbon active zones and ribbon unanchoring from synaptic tethers have been observed in
566 synaptopathic ears (Moverman et al., 2023; Lu et al., 2024; Mohamad et al., 2024). Though their
567 function is unclear, these structures persist into adulthood (Michanski et al., 2019; Hua et al.,
568 2021) and are a hallmark of cochlear aging (Stamataki et al., 2006), with larger ribbons being
569 associated with increased exocytotic activity (Jeng et al., 2020). Notably, noise exposure has also
570 been associated with enhanced exocytosis in IHCs, along with an increase in tone-burst
571 responses in auditory nerve fibers (Boero et al., 2021; Suthakar and Liberman, 2021).

572 In α9KO mice, ABR and DPOAE thresholds were elevated one week post-exposure at
573 P15, consistent with prior findings at P21 (Boero et al., 2018). However, unlike WT, ABR
574 thresholds in α9KOs nearly fully recovered by two months. DPOAE thresholds also normalized
575 except at 16 kHz, matching a slight, non-significant ABR threshold elevation at that frequency.
576 The recovery of ABR thresholds observed in α9KO mice, unlike the persistent elevation in WT
577 mice, may stem from reduced auditory sensitivity at hearing onset in α9KO mice, leading to less

578 effective noise exposure and milder impact. Despite threshold recovery, reduced wave 1
579 amplitudes and synapse counts suggest lasting damage to high-threshold, low-spontaneous-rate
580 fibers (Furman et al., 2013; Reijntjes et al., 2025). Additionally, noise-exposed α9KO ears showed
581 reduced sizes of pre- and postsynaptic puncta, indicating structural synaptic alterations. At P16
582 (one day post- exposure), ABR and DPOAE thresholds in both WT and α9KO mice were slightly
583 reduced compared to P15 and aligned with those of unexposed controls, suggesting that noise
584 had no immediate impact on auditory maturation at this stage. In contrast, Boero et al. (2021)
585 reported lasting damage in C57BL/6J mice one day after 120 dB SPL at P15, highlighting that
586 early noise effects depend on complex interactions between factors such as intensity, duration,
587 and genetic background, and differ from outcomes seen with noise exposure at mature stages.
588 Unlike WT and α9KO mice, α9KI mice showed no threshold shifts or synaptopathy after
589 noise, consistent with prior reports in mature α9KI mice (Taranda et al., 2009; Boero et al., 2018)
590 and recent gene therapy studies supporting protective effects of enhanced α9α10 nAChR activity
591 (Zhang et al., 2023; Slika et al., 2025). The protective role of the MOC system has been
592 recognized for decades: efferent stimulation reduces threshold shifts (Rajan, 1988; Reiter and
593 Liberman, 1995), while surgical de-efferentation increases vulnerability (Kujawa and Liberman,
594 1997). Overexpressing wild-type α9 also confers greater resistance to noise (Maison et al., 2002).
595 *In vivo* studies show that ACh evokes fast (~100ms) and slow (~10s) MOC effects on cochlear
596 responses (Sridhar et al., 1995, 1997; Cooper and Guinan, 2003). Fast suppression involves SK2-
597 mediated OHC hyperpolarization, while slow suppression likely reflects Ca^{2+} signaling and
598 increased OHC stiffness, both reducing cochlear vibrations (Cooper and Guinan, 2003). Evidence
599 suggests that efferent protection likely relies on slow, Ca^{2+}-dependent mechanisms that reduce
600 acoustic injury by dampening cochlear vibrations or altering OHC function via α9α10 receptor-
601 mediated Ca^{2+} influx (Reiter and Liberman, 1995; Maison et al., 2007). Though MOC-OHC
602 innervation is still maturing during early development (Simmons et al., 1996), our findings show

603 that enhanced α9α10 activity already confers robust protection against acoustic trauma.

Figures

Figure 1: Auditory function in WT, α9KO, and α9KI mice across different postnatal ages. (**a**) Representative ABR waveforms from WT (black), α9KI (red), and α9KO (blue) mice recorded at P14 in response to 16 kHz tone bursts at increasing sound pressure levels (dB SPL). Thresholds, defined by the presence of wave 1, are marked by green dashed traces. Waves 1, 2 and 3 are indicated by gray arrows. The scale bar applies to all three recordings. (**b**) Mean ABR thresholds from P12 to P75 in WT (P12 to P14 n = 9 and P15 to P75 n = 14), α9KO (P12 to P14 n = 7 and P15 to P75 n = 11), and α9KI (P12 to P14 n = 9 and P15 to P75 n = 12) mice at 11.33, 16, and 22.65 kHz. ABR waveforms first became detectable at P13 in α9KI mice, at P14 in WT mice, and between P14 and P15 in α9KO mice. (**c**) Mean DPOAE thresholds from P12 to P75 in WT (P12 to P14 n = 9 and P15 to P75 n = 14), α9KO (P12 to P14 n = 7 and P15 to P75 n = 11) and α9KI (P12 to P14 n = 9 and P15 to P75 n = 12) mice at 11.33, 16 and 22.65 kHz. DPOAE thresholds showed the same trend as ABR only at 11.33 kHz. Group means ± SEM are shown. Red asterisks represent the statistical significance of α9KI compared with WT**,** and blue asterisks represent the statistical significance of α9KO compared with WT (Kruskal-Wallis followed by post hoc Dunn test, *p < 0.05).

Figure 2: Suprathreshold ABR Wave1 amplitudes and latencies in WT, α9KO, and α9KI mice during postnatal development. (**a**) Representative examples of ABR waveforms recorded at 16 kHz, 80 dB SPL, from WT (black), α9KI (red), and α9KO (blue) mice. Waves 1, 2 and 3 are indicated by gray arrows. Each column illustrates waveform maturation across developmental stages (P12–P16, P22, P75) for each genotype. At P13, α9KI mice exhibit measurable responses, while distinct ABR waves emerge in WT and α9KO mice by P14. Waveform morphology stabilizes by P22 and remains consistent through P75. Scale bars apply to all traces. (**b**) ABR wave 1 amplitudes (μV) at 80 dB SPL for 11.33, 16, and 22.65 kHz across developmental ages in WT, α9KO, and α9KI mice. Amplitudes were measured as the difference between the maximum and minimum peaks. No values are shown for P12 due to the absence of discernible waves. (**c**) ABR wave 1 latencies (ms) at the same frequencies. A developmental decrease in latency is observed between P14 and P15 in all genotypes, though not statistically significant. The number of animals per genotype is the same as in Figure 1. Data represent mean ± SEM. Red asterisks denote significant differences between α9KI and WT; blue asterisks indicate significant differences between α9KO and WT (one-way ANOVA followed by Holm-Sidak test, *p < 0.05; **p < 0.01).

Figure 3: ABR wave 1 threshold measurements in control and noise-exposed WT, α9KO, and α9KI mice at different postnatal ages. ABR thresholds before and after exposure to noise at P15 in WT ($n_{control}$ = 14 and $n_{Exposed}$ = 12) (**a**), α9KO ($n_{control}$ = 11 and $n_{Exposed}$ = 11) (**b**), and α9KI ($n_{control}$ = 12 and $n_{Exposed}$ = 12) (**c**) mice at 8, 16 and 22.65 kHz. WT mice showed a significant increase in ABR thresholds 1 week and 2 months after exposure to noise, indicating a permanent threshold elevation. A recovery of ABR thresholds was observed in α9KO mice 2 months after exposure to noise. α9KI mice did not present any changes in ABR thresholds at any time after acoustic trauma. Each point represents the mean ± SEM. Asterisks represent the statistical significance (Mann-Whitney test, *p < 0.05; **p < 0.01).

Figure 4: Suprathreshold response amplitude for ABR wave 1 after P15 noise exposure in WT, α9KO, and α9KI mice at different postnatal ages compared to unexposed controls. ABR wave 1 amplitudes (in μV) at 80 dB SPL at 8, 16 and 22.65 kHz in WT ($n_{Control}$ = 14 and $n_{Exposed}$ = 12) (**a**), α9KO ($n_{Control}$ = 11 and $n_{Exposed}$ = 11) (**b**), and α9KI ($n_{Control}$ = 12 and $n_{Exposed}$ = 12) (**c**) mice at the same time points shown in Figure 3. Each panel inset displays representative ABR waveforms recorded at 80 dB SPL for the corresponding frequency, shown for all groups at P75. Scale bars (1 μV vertical, 1 ms horizontal) apply to all traces. WT and α9KO mice exhibited reduced ABR wave 1 amplitudes following noise exposure, whereas wave 1 amplitudes in α9KI mice remained unaffected. Data are presented as mean ± SEM. Statistical significance is indicated by asterisks (Mann-Whitney test, *p < 0.05; **p < 0.01).

Figure 5: **Assessment of OHC functional integrity at different postnatal ages following noise exposure at P15 in WT, α9KO, and α9KI mice.** DPOAE thresholds are shown for WT ($n_{Control}$ = 14 and $n_{Exposed}$ = 12) (**a**), α9KO ($n_{Control}$ = 11 and $n_{Exposed}$ = 11) (**b**), and α9KI ($n_{Control}$ = 12 and $n_{Exposed}$ = 12) (**c**) at 8, 16 and 22.65 kHz. WT mice exhibited a transient increase in DPOAE thresholds 1 week post-exposure at 16 kHz. α9KO mice showed increased thresholds at 8 and 16 kHz 1 week post-exposure, with sustained elevation at 16 kHz up to 2 months. α9KI mice demonstrated no changes in DPOAE thresholds after noise exposure. Data are presented as mean ± SEM. Statistical significance is indicated by asterisks (Mann-Whitney test, *p < 0.05; **p < 0.01).

Figure 6: Analysis of IHC ribbon synapses in unexposed WT, α9KO, and α9KI mice at P15 and P75. (**a**) Representative confocal images of IHC synapses at the apex of the cochlea from cochleae immunolabeled for presynaptic ribbons (CtBP2-red) and postsynaptic receptor patches (GluA2-green) for WT (left), α9KO (middle) and α9KI (right) at P15 and P75. CtBP2 antibody also weakly stains IHC nuclei. Scale bar, 7 μm. (**b**) Quantification of putative ribbon synapses per IHC (i.e., colocalized CtBP2 and GluA2 puncta). WT P15: n_{Apex} = 182 IHC, n_{Middle} = 248, n_{Base} = 68 (6 animals); WT P75: n_{Apex} = 80 IHC, n_{Middle} = 75, n_{Base} = 60 IHC (14 animals); α9KO P15: n_{Apex} = 201 IHC, n_{Middle} = 230, n_{Base} = 164 (5 animals); α9KO P75: n_{Apex} = 100 IHC, n_{Middle} = 84, n_{Base} = 118 (11 animals); α9KI P15: n_{Apex} = 155 IHC, n_{Middle} = 284, n_{Base} = 85 (5 animals) and α9KI P75: n_{Apex} = 178 IHC, n_{Middle} = 319, n_{Base} = 198 (12 animals). (**c**) Volumes of fluorescence staining for ribbons (CtBP2 size) and (**d**) AMPA receptors (GluA2 size) for each of the synaptic pairs (WT P15: n_{Apex} = 684 synaptic pairs, n_{Middle} = 729, n_{Base} = 380; WT P75: n_{Apex} = 450, n_{Middle} = 509, n_{Base} = 203; α9KO P15: n_{Apex} = 845, n_{Middle} = 800, n_{Base} = 735; α9KO P75: n_{Apex} = 367, n_{Middle} = 187, n_{Base} = 221; α9KI P15: n_{Apex} = 428, n_{Middle} = 484, n_{Base} = 232 and α9KI P75: n_{Apex} = 247, n_{Middle} = 270, n_{Base} = 240). Violin plots indicate median (solid line) and interquartile range (IQR, dashed lines). Asterisks denote statistical significance. The number of synapses was analyzed using the Kruskal–Wallis

test followed by Dunn's post-test, while synaptic volumes were analyzed using one-way ANOVA followed by the Holm–Sidak test.; *p < 0.05; **p < 0.01; ***p < 0.001, ****p < 0.0001).

Figure 7: Analysis of the degree of IHC synaptopathy two months after exposure to noise at P15. Left, Representative confocal images of IHC synapses at the apex of the cochlea from cochleae immunolabeled for presynaptic ribbons (CtBP2-red), postsynaptic receptor patches (GluA2-green) and IHCs (Myosin VIIa-blue). CtBP2 antibody also weakly stains IHC nuclei. Scale bar, 10µm. Right, Quantitative data obtained from WT, α9KO, and α9KI mice at P75. For each IHC, we analyzed the number of CtBP2 puncta, postsynaptic GluA2 receptor patches, and putative ribbon synapses. (**a**) In traumatized WT mice, there was a reduction in the number of CtBP2 puncta, GluA2 receptor patches, and putative synapse, at the apical and basal region of the cochlea (WT Control: n_{Apex} = 80 IHC, n_{Middle} = 75, n_{Base}= 60; WT Exposed: n_{Apex} = 82 IHC, n_{Middle} = 90, n_{Base} = 50). (**b**) In traumatized α9KO mice, there was a reduction in the number of prelocalized, postlocalized, and colocalized puncta depending on cochlear frequency/location (α9KO Control: n_{Apex} = 100 IHC, n_{Middle} = 84, n_{Base} = 118; α9KO Exposed: n_{Apex} = 234 IHC, n_{Middle} = 60, n_{Base} = 90). (**c**) In traumatized α9KI mice, no difference was found in the number of presynaptic ribbons, postsynaptic AMPA receptors, and colocalization puncta for the three regions of the cochlea (α9KI Control: n_{Apex} = 178 IHC, n_{Middle} = 319, n_{Base} = 198; α9KI Exposed: n_{Apex} = 196 IHC, n_{Middle} = 145, n_{Base} = 80). Violin plots indicate median (solid line) and IQR (dashed lines). Asterisks denote the statistical significance (Mann Whitney test, **p < 0.01; ***p < 0.001, ****p < 0.0001).

Figure 8: Volumes of presynaptic ribbons and postsynaptic receptor patches for each synaptic pair from control and noise-exposed WT, α9KO and α9KI mice. Violin plots comparing the volumes of fluorescence staining for ribbons (CtBP2 size) and AMPA receptors (GluA2 size) between control and noise-exposed mice. The quantification was made in the apex, middle and base regions of the cochlea from WT (**a**) (Control: n_{Apex} = 450 synaptic pairs, n_{Middle} = 509, n_{Base} = 203; Exposed: n_{Apex} = 497 synaptic pairs, n_{Middle} = 175, n_{Base} = 250); α9KO (**b**) (Control: n_{Apex} = 367 synaptic pairs, n_{Middle} = 187, n_{Base} = 221; Exposed: n_{Apex} = 207 synaptic pairs, n_{Middle} = 300, n_{Base} = 145) and α9KI (**c**) (Control: n_{Apex} = 247 synaptic pairs, n_{Middle} = 270, n_{Base} = 240; Exposed: n_{Apex} = 280 synaptic pairs, n_{Middle} = 310, n_{Base} = 360) mice. Violin plots indicate median (solid line) and IQR (dashed lines). Asterisks denote the statistical significance (t-test; *p < 0.05; ***p < 0.001).

References

Antoli-Candela FJ, Kiang N (1978) Unit activity underlying the N1 potential. In: Evoked electrical activity in the auditory nervous system (Naunton R, Fernandez C, eds), pp 165–191.

Babola TA, Li S, Wang Z, Kersbergen CJ, Elgoyhen AB, Coate TM, Bergles DE (2021) Purinergic Signaling Controls Spontaneous Activity in the Auditory System throughout Early Development. J Neurosci 41:594–612.

Boero LE, Castagna VC, Di Guilmi MN, Goutman JD, Elgoyhen AB, Gómez-Casati ME (2018) Enhancement of the medial olivocochlear system prevents hidden hearing loss. The Journal of Neuroscience 38:7440–7451 Available at: http://www.jneurosci.org/lookup/doi/10.1523/JNEUROSCI.0363-18.2018.

Boero LE, Payne S, Gómez-Casati ME, Rutherford MA, Goutman JD (2021) Noise Exposure Potentiates Exocytosis From Cochlear Inner Hair Cells. Front Synaptic Neurosci 13:740368.

Buchwald JS, Huang CM (1975) Far-field acoustic response: Origins in the cat. Science 189:382–384.

Caminos C, Vale E, Lujan R, Martinez-Galan JR, Juiz JM (2005) Developmental regulation and adult maintenance of potassium channel proteins (Kv 1.1 and Kv 1.2) in the cochlear nucleus of the rat. Brain research 1056 Available at: https://pubmed.ncbi.nlm.nih.gov/16122713/ [Accessed October 16, 2024].

Chang EF, Merzenich MM (2003) Environmental noise retards auditory cortical development. Science 300:498–502.

Clause A, Kim G, Sonntag M, Weisz CJC, Vetter DE, Rűbsamen R, Kandler K (2014) The precise temporal pattern of prehearing spontaneous activity is necessary for tonotopic map refinement. Neuron 82:822–835.

Cooper NP, Guinan JJ (2003) Separate mechanical processes underlie fast and slow effects of medial olivocochlear efferent activity. J Physiol 548:307–312.

Davis RR, Kozel P, Erway LC (2003) Genetic influences in individual susceptibility to noise: a review. Noise Health 5:19–28.

De Faveri F, Ceriani F, Marcotti W (2025) In vivo spontaneous Ca2+ activity in the pre-hearing mammalian cochlea. Nat Commun 16:29 Available at: https://www.ncbi.nlm.nih.gov/pmc/articles/PMC11695946/ [Accessed April 4, 2025].

Di Guilmi MN, Boero LE, Castagna VC, Rodríguez-Contreras A, Wedemeyer C, Gómez-Casati ME, Elgoyhen AB (2019) Strengthening of the efferent olivocochlear system leads to synaptic dysfunction and tonotopy disruption of a central auditory nucleus. The Journal of Neuroscience:2536–18.

Dorrn AL, Yuan K, Barker AJ, Schreiner CE, Froemke RC (2010) Developmental sensory experience balances cortical excitation and inhibition. Nature 465:932–936.

Dulon D, Lenoir M (1996) Cholinergic responses in developing outer hair cells of the rat cochlea. Eur J Neurosci 8:1945–1952.

Ernfors P, Kucera J, Lee KF, Loring J, Jaenisch R (1995) Studies on the physiological role of brain-derived neurotrophic factor and neurotrophin-3 in knockout mice. Int J Dev Biol 39:799–807 Available at: http://www.ncbi.nlm.nih.gov/entrez/query.fcgi?cmd=Retrieve&db=PubMed&dopt=Citation&list_uids=8645564.

Fernandez KA, Jeffers PWC, Lall K, Liberman MC, Kujawa SG (2015) Aging after noise exposure : Acceleration of cochlear synaptopathy in " recovered " ears. The Journal of Neuroscience 35:7509–7520.

Frank T, Khimich D, Neef A, Moser T (2009) Mechanisms contributing to synaptic Ca2+ signals and their heterogeneity in hair cells. Proc Natl Acad Sci U S A 106:4483–4488.

Friauf E, Lohmann C (1999) Development of auditory brainstem circuitry. Activity-dependent and activity-independent processes. Cell Tissue Res 297:187–195.

Froemke RC, Jones BJ (2011) Development of auditory cortical synaptic receptive fields. Neurosci Biobehav Rev 35:2105–2113.

Furman AC, Kujawa SG, Liberman MC (2013) Noise-induced cochlear neuropathy is selective for fibers with low spontaneous rates. Journal of Neurophysiology 110:577–586.

Gilels F, Paquette ST, Zhang J, Rahman I, White PM (2013) Mutation of foxo3 causes adult onset auditory neuropathy and alters cochlear synapse architecture in mice. Journal of Neuroscience 33:18409–18424.

Glowatzki E, Fuchs PA (2000) Cholinergic synaptic inhibition of inner hair cells in the neonatal mammalian cochlea. Science 288:2366–2368.

Gomez-Casati ME, Fuchs PA, Elgoyhen AB and, Katz E (2005) Biophysical and pharmacological characterization of nicotinic cholinergic receptors in rat cochlear inner hair cells. Journal of Physiology 566:103–118 Available at: http://www.pubmedcentral.nih.gov/articlerender.fcgi?artid=1464719&tool=pmcentrez&rendertype=abstract [Accessed August 10, 2013].

Goutman JD, Fuchs PA, Glowatzki E (2005) Facilitating efferent inhibition of inner hair cells in the cochlea of the neonatal rat. Journal of Physiology 566:49–59 Available at: http://www.pubmedcentral.nih.gov/articlerender.fcgi?artid=1464729&tool=pmcentrez&rendertype=abstract [Accessed August 31, 2013].

He DZ, Dallos P (1999) Development of acetylcholine-induced responses in neonatal gerbil outer hair cells. J Neurophysiol 81:1162–1170.

Hirtz JJ, Boesen M, Braun N, Deitmer JW, Kramer F, Lohr C, Müller B, Nothwang HG, Striessnig J, Löhrke S, Friauf E (2011) Cav1.3 calcium channels are required for normal development of the auditory brainstem. J Neurosci 31:8280–8294.

790 Hua Y, Ding X, Wang H, Wang F, Lu Y, Neef J, Gao Y, Moser T, Wu H (2021) Electron
791 Microscopic Reconstruction of Neural Circuitry in the Cochlea. Cell Rep 34:108551.

792 Jeng JY, Ceriani F, Olt J, Brown SDM, Holley MC, Bowl MR, Johnson SL, Marcotti W (2020)
793 Pathophysiological changes in inner hair cell ribbon synapses in the ageing mammalian
794 cochlea. Journal of Physiology 598:4339–4355.

795 Jensen JB, Lysaght AC, Liberman MC, Qvortrup K, Stankovic KM (2015) Immediate and delayed
796 cochlear neuropathy after noise exposure in pubescent mice. PLoS ONE 10:1–17.

797 Jing Z, Rutherford MA, Takago H, Frank T, Fejtova A, Khimich D, Moser T, Strenzke N (2013)
798 Disruption of the presynaptic cytomatrix protein bassoon degrades ribbon anchorage,
799 multiquantal release, and sound encoding at the hair cell afferent synapse. Journal of
800 Neuroscience 33:4456–4467.

801 Johnson SL, Eckrich T, Kuhn S, Zampini V, Franz C, Ranatunga KM, Roberts TP, Masetto S,
802 Knipper M, Kros CJ, Marcotti W (2011) Position-dependent patterning of spontaneous
803 action potentials in immature cochlear inner hair cells. Nat Neurosci 14:711–717.

804 Johnson SL, Wedemeyer C, Vetter DE, Adachi R, Holley MC, Elgoyhen AB, Marcotti W (2013)
805 Cholinergic efferent synaptic transmission regulates the maturation of auditory hair cell
806 ribbon synapses. Open Biology 3.

807 Karplus M, Lee C, Cashore WJ, Oh W (1988) The effects of brain bilirubin deposition on auditory
808 brain stem evoked responses in rats. Early Hum Dev 16:185–194.

809 Katz E, Elgoyhen AB, Gómez-Casati ME, Knipper M, Vetter DE, Fuchs P a, Glowatzki E, Gomez-
810 Casati ME, Knipper M, Vetter DE, Fuchs P a, Glowatzki E, Bele A, Knipper M, Vetter DE,
811 Fuchs P a (2004) Developmental regulation of nicotinic synapses on cochlear inner hair
812 cells. J Neurosci 24:7814–7820 Available at:
813 http://www.ncbi.nlm.nih.gov/entrez/query.fcgi?cmd=Retrieve&db=PubMed&dopt=Citation
814 &list_uids=15356192 [Accessed August 31, 2013].

815 Keuroghlian AS, Knudsen EI (2007) Adaptive auditory plasticity in developing and adult animals.
816 Prog Neurobiol 82:109–121.

817 Khimich D, Nouvian R, Pujol R, Tom Dieck S, Egner A, Gundelfinger ED, Moser T (2005) Hair
818 cell synaptic ribbons are essential for synchronous auditory signalling. Nature 434:889–
819 894 Available at:
820 http://www.ncbi.nlm.nih.gov/entrez/query.fcgi?cmd=Retrieve&db=PubMed&dopt=Citation
821 &list_uids=15829963.

822 Kim SE, Turkington K, Kushmerick C, Kim JH (2013) Central dysmyelination reduces the temporal
823 fidelity of synaptic transmission and the reliability of postsynaptic firing during high-
824 frequency stimulation. J Neurophysiol 110:1621–1630.

825 Knipper M, Zimmermann U, Rohbock K, Kopschall I, Zenner HP (1995) Synaptophysin and GAP-
826 43 proteins in efferent fibers of the inner ear during postnatal development. Brain Res Dev
827 Brain Res 89:73–86 Available at:
828 http://www.ncbi.nlm.nih.gov/entrez/query.fcgi?cmd=Retrieve&db=PubMed&dopt=Citation
829 &list_uids=8575095.

Kujawa SG, Liberman MC (1997) Conditioning-related protection from acoustic injury: Effects of chronic deefferentation and sham surgery. Journal of Neurophysiology 78:3095–3106.

Kujawa SG, Liberman MC (2009) Adding insult to injury: cochlear nerve degeneration after "temporary" noise-induced hearing loss. J Neurosci 29:14077–14085 Available at: http://www.ncbi.nlm.nih.gov/pubmed/19906956%5Cnhttp://www.pubmedcentral.nih.gov/articlerender.fcgi?artid=PMC2812055.

Lauer AM, May BJ, Ay BRJM, Lauer AM, May BJ (2011) The medial olivocochlear system attenuates the developmental impact of early noise exposure. JARO - Journal of the Association for Research in Otolaryngology 12:329–343 Available at: http://www.ncbi.nlm.nih.gov/entrez/query.fcgi?cmd=Retrieve&db=PubMed&dopt=Citation&list_uids=21347798.

Leake PA, Hradek GT, Chair L, Snyder RL (2006) Neonatal deafness results in degraded topographic specificity of auditory nerve projections to the cochlear nucleus in cats. J Comp Neurol 497:13–31.

Liberman LD, Wang H, Liberman MC (2011) Opposing gradients of ribbon size and AMPA receptor expression underlie sensitivity differences among cochlear-nerve/hair-cell synapses. The Journal of neuroscience : the official journal of the Society for Neuroscience 31:801–808 Available at: http://www.pubmedcentral.nih.gov/articlerender.fcgi?artid=3290333&tool=pmcentrez&rendertype=abstract [Accessed August 31, 2013].

Liberman MC (1991) The olivocochlear efferent bundle and susceptibility of the inner ear to acoustic injury. J Neurophysiol 65:123–132 Available at: http://www.ncbi.nlm.nih.gov/entrez/query.fcgi?cmd=Retrieve&db=PubMed&dopt=Citation&list_uids=1999726.

Lippe WR (1994) Rhythmic spontaneous activity in the developing avian auditory system. J Neurosci 14:1486–1495 Available at: http://www.ncbi.nlm.nih.gov/entrez/query.fcgi?cmd=Retrieve&db=PubMed&dopt=Citation&list_uids=8126550.

Lu Y, Liu J, Li B, Wang H, Wang F, Wang S, Wu H, Han H, Hua Y (2024) Spatial patterns of noise-induced inner hair cell ribbon loss in the mouse mid-cochlea. iScience 27:108825.

Maison SF, Liberman MC (2000) Predicting Vulnerability to Acoustic Injury with a Noninvasive Assay of Olivocochlear Reflex Strength. The Journal of neuroscience 20:4701–4707.

Maison SF, Luebke AE, Liberman MC, Zuo J (2002) Efferent protection from acoustic injury is mediated via alpha9 nicotinic acetylcholine receptors on outer hair cells. J Neurosci 22:10838-46.

Maison SF, Parker LL, Young L, Adelman JP, Zuo J, Liberman MC (2007) Overexpression of SK2 Channels Enhances Efferent Suppression of Cochlear Responses without Enhancing Noise Resistance. Journal of neurophysiology 97:2930 Available at: https://pmc.ncbi.nlm.nih.gov/articles/PMC1850627/ [Accessed June 5, 2025].

Maison SF, Usubuchi H, Liberman MC (2013) Efferent feedback minimizes cochlear neuropathy from moderate noise exposure. Journal of Neuroscience 33:5542–5552.

Marcotti W, Johnson SL, Kros CJ (2004) A transiently expressed SK current sustains and modulates action potential activity in immature mouse inner hair cells. J Physiol Available at: http://www.ncbi.nlm.nih.gov/entrez/query.fcgi?cmd=Retrieve&db=PubMed&dopt=Citation&list_uids=15331671.

Marcotti W, Johnson SL, Rusch A, Kros CJ (2003) Sodium and calcium currents shape action potentials in immature mouse inner hair cells. J Physiol 552:743–761 Available at: http://www.ncbi.nlm.nih.gov/entrez/query.fcgi?cmd=Retrieve&db=PubMed&dopt=Citation&list_uids=12937295.

Matsubara A, Laake JH, Davanger S, Usami S, Ottersen OP (1996) Organization of AMPA receptor subunits at a glutamate synapse: a quantitative immunogold analysis of hair cell synapses in the rat organ of Corti. The Journal of Neuroscience 16:4457–4467.

Melcher J, Kiang NY (1996) Generators of the brainstem auditory evoked potential in cat. III: Identified cell populations. Hearing research 93:52–71 Available at: https://pubmed.ncbi.nlm.nih.gov/8735068/ [Accessed November 1, 2021].

Michanski S, Smaluch K, Maria Steyer A, Chakrabarti R, Setz C, Oestreicher D, Fischer C, Möbius W, Moser T, Vogl C, Wichmann C (2019) Mapping developmental maturation of inner hair cell ribbon synapses in the apical mouse cochlea. Proceedings of the National Academy of Sciences of the United States of America 116:6415–6424.

Moglie MJ, Fuchs PA, Elgoyhen AB, Goutman JD (2018) Compartmentalization of antagonistic Ca2+ signals in developing cochlear hair cells. Proc Natl Acad Sci U S A 115:E2095–E2104.

Mohamad NI, Santra P, Park Y, Matthews IR, Taketa E, Chan DK (2024) Synaptic ribbon dynamics after noise exposure in the hearing cochlea. Commun Biol 7:421.

Mostafapour SP, Cochran SL, Del Puerto NM, Rubel EW (2000) Patterns of cell death in mouse anteroventral cochlear nucleus neurons after unilateral cochlea removal. J Comp Neurol 426:561–571.

Moverman DJ, Liberman LD, Kraemer S, Corfas G, Liberman MC (2023) Ultrastructure of noise-induced cochlear synaptopathy. Sci Rep 13:19456.

Müller M M, von Hunerbein K, Hoidis S, Smolders JW (2005) A physiological place-frequency map of the cochlea in the CBA/J mouse. Hear Res 202:63–73 Available at: http://www.ncbi.nlm.nih.gov/entrez/query.fcgi?cmd=Retrieve&db=PubMed&dopt=Citation&list_uids=15811700.

Müller M, Smolders JW (2005) Shift in the cochlear place-frequency map after noise damage in the mouse. NeuroReport 16:1183–1187 Available at: http://www.ncbi.nlm.nih.gov/entrez/query.fcgi?cmd=Retrieve&db=PubMed&dopt=Citation&list_uids=16012345.

908 Ollion J, Cochennec J, Loll F, Escudé C, Boudier T (2013) TANGO: A generic tool for high-
909 throughput 3D image analysis for studying nuclear organization. Bioinformatics 29:1840–
910 1841.

911 Özçete ÖD, Moser T (2021) A sensory cell diversifies its output by varying Ca2+ influx-release
912 coupling among active zones. EMBO J 40:e106010.

913 Paquette ST, Gilels F, White PM (2016) Noise exposure modulates cochlear inner hair cell ribbon
914 volumes, correlating with changes in auditory measures in the FVB/nJ mouse. Scientific
915 Reports 6:1–13 Available at: http://dx.doi.org/10.1038/srep25056.

916 Pujol R (1985) Morphology, synaptology and electrophysiology of the developing cochlea. Acta
917 Otolaryngol Suppl 421:5-9.

918 Pujol R, Carlier E, Devigne C (1978) Different patterns of cochlear innervation during the
919 development of the kitten. J Comp Neurol 177:529-36.

920 Rajan R (1988) Effect of electrical stimulation of the crossed olivocochlear bundle on temporary
921 threshold shifts in auditory sensitivity. I . Dependence on electrical stimulation parameters.
922 J Neurophysiol 60:549–568.

923 Reijntjes DOJ, Burke K, Paul S, Mueller U, Glowatzki E, Lauer AM (2025) Increased vulnerability
924 to noise exposure of low spontaneous rate type 1C spiral ganglion neuron synapses with
925 inner hair cells (Pre-Print). bioRxiv:2025.05.19.654865.

926 Reiter ER, Liberman MC (1995) Efferent-mediated protection from acoustic overexposure:
927 relation to slow effects of olivocochlear stimulation. Journal of neurophysiology 73:506–
928 514.

929 Robles L, Ruggero MA (2001) Mechanics of the mammalian cochlea. Physiological reviews
930 81:1305–1352.

931 Roux I, Wersinger E, McIntosh JM, Fuchs P a, Glowatzki E (2011) Onset of cholinergic efferent
932 synaptic function in sensory hair cells of the rat cochlea. The Journal of neuroscience : the
933 official journal of the Society for Neuroscience 31:15092–15101 Available at:
934 http://www.pubmedcentral.nih.gov/articlerender.fcgi?artid=3213862&tool=pmcentrez&re
935 ndertype=abstract [Accessed August 10, 2013].

936 Rybalko N, Chumak T, Bureš Z, Popelář J, Šuta D, Syka J (2015) Development of the acoustic
937 startle response in rats and its change after early acoustic trauma. Behav Brain Res
938 286:212–221.

939 Sage D, Donati L, Soulez F, Fortun D, Schmit G, Seitz A, Guiet R, Vonesch C, Unser M (2017)
940 DeconvolutionLab2: An open-source software for deconvolution microscopy. Methods
941 115:28–41 Available at: http://dx.doi.org/10.1016/j.ymeth.2016.12.015.

942 Sanes DH, Bao S (2009) Tuning up the developing auditory CNS. Curr Opin Neurobiol 19:188–
943 199 Available at:
944 http://www.ncbi.nlm.nih.gov/entrez/query.fcgi?cmd=Retrieve&db=PubMed&dopt=Citation
945 &list_uids=19535241.

946 Sanes DH, Walsh EJ (1998) The development of central auditory processing. In: Development
947 of the Auditory System (Rubel EW, Popper AN, Fay RR, eds), pp 271–314. New York:
948 Springer.

949 Schindelin J, Arganda-Carreras I, Frise E, Kaynig V, Longair M, Pietzsch T, Preibisch S, Rueden
950 C, Saalfeld S, Schmid B, Tinevez J-Y, White DJ, Hartenstein V, Eliceiri K, Tomancak P,
951 Cardona A (2012) Fiji: an open-source platform for biological-image analysis. Nature
952 methods 9:676–682.

953 Schrode KM, Dent ML, Lauer AM (2022) Sources of variability in auditory brainstem response
954 thresholds in a mouse model of noise-induced hearing loss. J Acoust Soc Am 152:3576–
955 3582 Available at: https://www.ncbi.nlm.nih.gov/pmc/articles/PMC9756347/ [Accessed
956 May 16, 2024].

957 Shapiro SM (1988) Acute brainstem auditory evoked potential abnormalities in jaundiced Gunn
958 rats given sulfonamide. Pediatr Res 23:306–310.

959 Shaw NA (1988) The auditory evoked potential in the rat--a review. Prog Neurobiol 31:19–45.

960 Sheets L, Kindt KS, Nicolson T (2012) Presynaptic CaV1.3 channels regulate synaptic ribbon size
961 and are required for synaptic maintenance in sensory hair cells. J Neurosci 32:17273–
962 17286.

963 Shera CA, Guinan Jr. JJ (1999) Evoked otoacoustic emissions arise by two fundamentally
964 different mechanisms: a taxonomy for mammalian OAEs. J Acoust Soc Am 105:782–798.

965 Simmons DD, Mansdorf NB, Kim JH (1996) Olivocochlear innervation of inner and outer hair cells
966 during postnatal maturation: evidence for a waiting period. J Comp Neurol 370:551–562
967 Available at:
968 http://www.ncbi.nlm.nih.gov/entrez/query.fcgi?cmd=Retrieve&db=PubMed&dopt=Citation
969 &list_uids=8807454.

970 Simmons DD, Manson-Gieseke L, Hendrix TW, McCarter S (1990) Reconstructions of efferent
971 fibers in the postnatal hamster cochlea. Hear Res 49:127-39.

972 Slika E, Fuchs PA, Wood MB (2025) Virally mediated enhancement of efferent inhibition reduces
973 acoustic trauma in wild-type murine cochleas. Mol Ther Methods Clin Dev 33:101455
974 Available at: https://www.ncbi.nlm.nih.gov/pmc/articles/PMC11999434/ [Accessed May
975 29, 2025].

976 Song L, McGee J, Walsh EJ (2006) Frequency- and level-dependent changes in auditory
977 brainstem responses (ABRS) in developing mice. J Acoust Soc Am 119:2242–2257.

978 Sonntag M, Englitz B, Kopp-Scheinpflug C, Rübsamen R (2009) Early Postnatal Development of
979 Spontaneous and Acoustically Evoked Discharge Activity of Principal Cells of the Medial
980 Nucleus of the Trapezoid Body: An In Vivo Study in Mice. J Neurosci 29:9510–9520
981 Available at: https://www.ncbi.nlm.nih.gov/pmc/articles/PMC6666529/ [Accessed October
982 14, 2024].

983 Sridhar TS, Brown MC, Sewell WF (1997) Unique postsynaptic signaling at the hair cell efferent
984 synapse permits calcium to evoke changes on two time scales. Journal of Neuroscience
985 17:428–437.

986 Sridhar TS, Liberman MC, Brown MC, Sewell WF (1995) A novel cholinergic “slow effect” of
987 efferent stimulation on cochlear potentials in the guinea pig. J Neurosci 15:3667–3678.

988 Stamataki S, Francis HW, Lehar M, May BJ, Ryugo DK (2006) Synaptic alterations at inner hair
989 cells precede spiral ganglion cell loss in aging C57BL/6J mice. Hearing Research
990 221:104–118 Available at: http://www.ncbi.nlm.nih.gov/pubmed/17005343 [Accessed
991 August 31, 2013].

992 Sun YJ, Wu GK, Liu B-H, Li P, Zhou M, Xiao Z, Tao HW, Zhang LI (2010) Fine-tuning of pre-
993 balanced excitation and inhibition during auditory cortical development. Nature 465:927–
994 931.

995 Suthakar K, Liberman MC (2021) Auditory-Nerve Responses in Mice with Noise-Induced
996 Cochlear Synaptopathy. https://doi.org/101152/jn003422021 Available at:
997 https://journals.physiology.org/doi/abs/10.1152/jn.00342.2021 [Accessed November 24,
998 2021].

999 Taranda J, Maison SF, Ballestero JA, Katz E, Savino J, Vetter DE, Boulter J, Liberman MC, Fuchs
1000 PA, Elgoyhen AB (2009) A point mutation in the hair cell nicotinic cholinergic receptor
1001 prolongs cochlear inhibition and enhances noise protection. PLoS Biology 7:71–83.

1002 Tierney TS, Russell FA, Moore DR (1997) Susceptibility of developing cochlear nucleus neurons
1003 to deafferentation-induced death abruptly ends just before the onset of hearing. J Comp
1004 Neurol 378:295–306.

1005 Tritsch NX, Bergles DE (2010) Developmental regulation of spontaneous activity in the
1006 Mammalian cochlea. J Neurosci 30:1539–1550.

1007 Vattino LG, Wedemeyer C, Elgoyhen AB, Katz E (2020) Functional Postnatal Maturation of the
1008 Medial Olivocochlear Efferent–Outer Hair Cell Synapse. Journal of Neuroscience
1009 40:4842–4857.

1010 Vetter DE, Liberman MC, Mann J, Barhanin J, Boulter J, Brown MC, Saffiote-Kolman J,
1011 Heinemann SF, Elgoyhen AB (1999) Role of alpha9 nicotinic ACh receptor subunits in the
1012 development and function of cochlear efferent innervation. Neuron 23:93-103.

1013 Waguespack J, Salles FT, Kachar B, Ricci AJ (2007) Stepwise morphological and functional
1014 maturation of mechanotransduction in rat outer hair cells. J Neurosci 27:13890–13902.

1015 Walsh E, McGee J, McFadden S, Liberman M (1998) Long-term effects of sectioning the
1016 olivocochlear bundle in neonatal cats. JNeurosci 18:3859–3869.

1017 Wang Y, Sanghvi M, Gribizis A, Zhang Y, Song L, Morley B, Barson DG, Santos-Sacchi J,
1018 Navaratnam D, Crair M (2021) Efferent feedback controls bilateral auditory spontaneous
1019 activity. Nat Commun 12:2449 Available at:
1020 https://www.ncbi.nlm.nih.gov/pmc/articles/PMC8079389/ [Accessed March 7, 2024].

1021 Weisstaub N, Vetter DE, Elgoyhen AB, Katz E (2002) The alpha9alpha10 nicotinic acetylcholine
1022 receptor is permeable to and is modulated by divalent cations. Hear Res 167:122-35.

1023 Wheeler EF, Bothwell M, Schecterson LC, von Bartheld CS (1994) Expression of BDNF and NT-
1024 3 mRNA in hair cells of the organ of Corti: quantitative analysis in developing rats. Hear
1025 Res 73:46–56.

1026 Wong HC, Zhang Q, Beirl AJ, Petralia RS, Wang Y-X, Kindt K (2019) Synaptic mitochondria
1027 regulate hair-cell synapse size and function. eLife 8:e48914 Available at:
1028 https://www.ncbi.nlm.nih.gov/pmc/articles/PMC6879205/ [Accessed December 19, 2024].

1029 Zhang Y, Hiel H, Vincent PFY, Wood MB, Elgoyhen AB, Chien W, Lauer A, Fuchs PA (2023)
1030 Engineering olivocochlear inhibition to reduce acoustic trauma. Mol Ther Methods Clin
1031 Dev 29:17–31.

1032 Zhou X, Merzenich MM (2008) Enduring effects of early structured noise exposure on temporal
1033 modulation in the primary auditory cortex. Proc Natl Acad Sci U S A 105:4423–4428
1034 Available at: https://www.ncbi.nlm.nih.gov/pmc/articles/PMC2393777/ [Accessed May 13,
1035 2024].

1036
1037

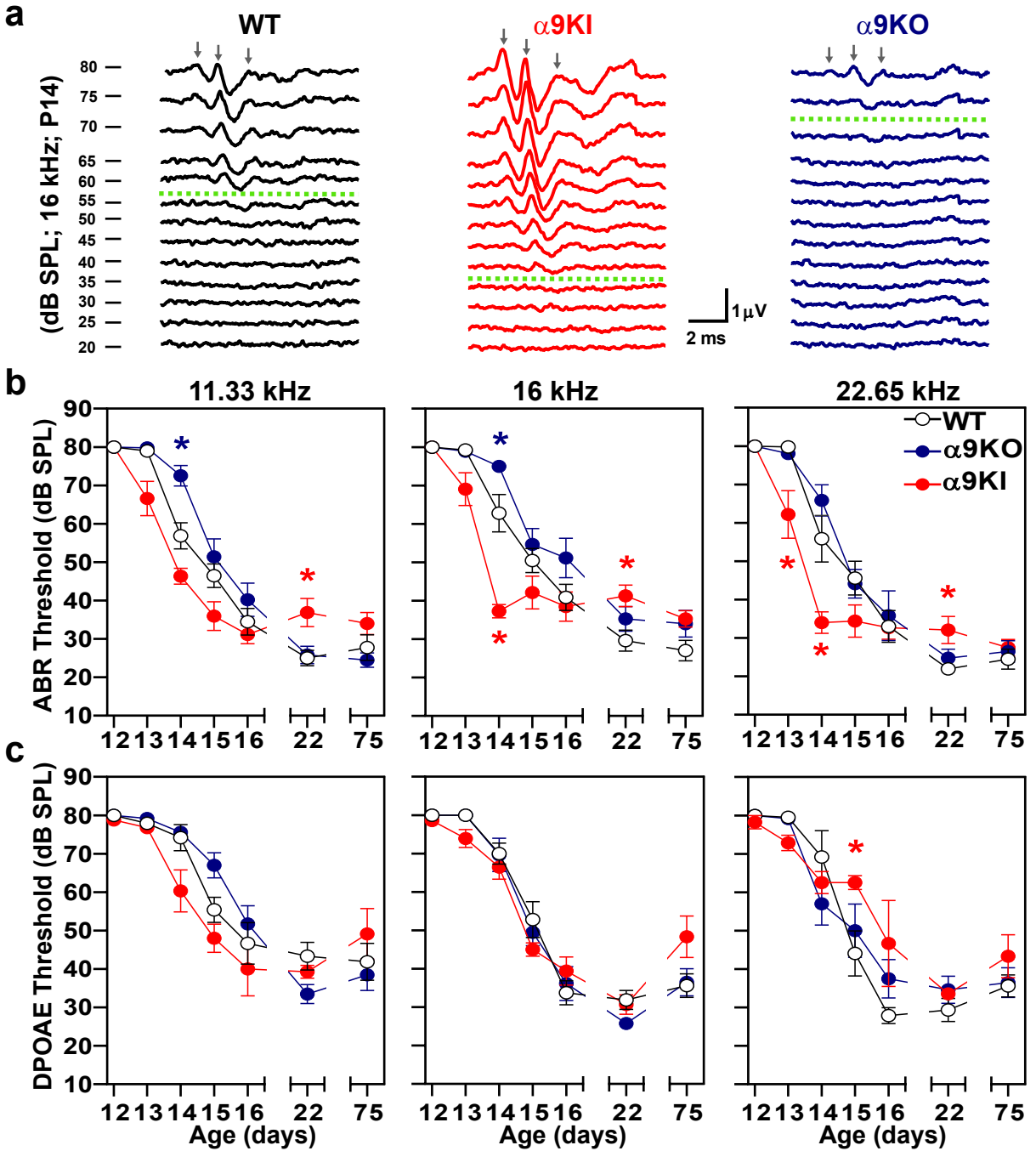
a
WT
α9KI
α9KO
(dB SPL; 16 kHz; P14)
80
75
70
65
60
55
50
45
40
35
30
25
20
1 μV
2 ms
b
11.33 kHz
16 kHz
22.65 kHz
WT
α9KO
α9KI
ABR Threshold (dB SPL)
90
80
70
60
50
40
30
20
10
12 13 14 15 16 22 75
c
DPOAE Threshold (dB SPL)
Age (days)

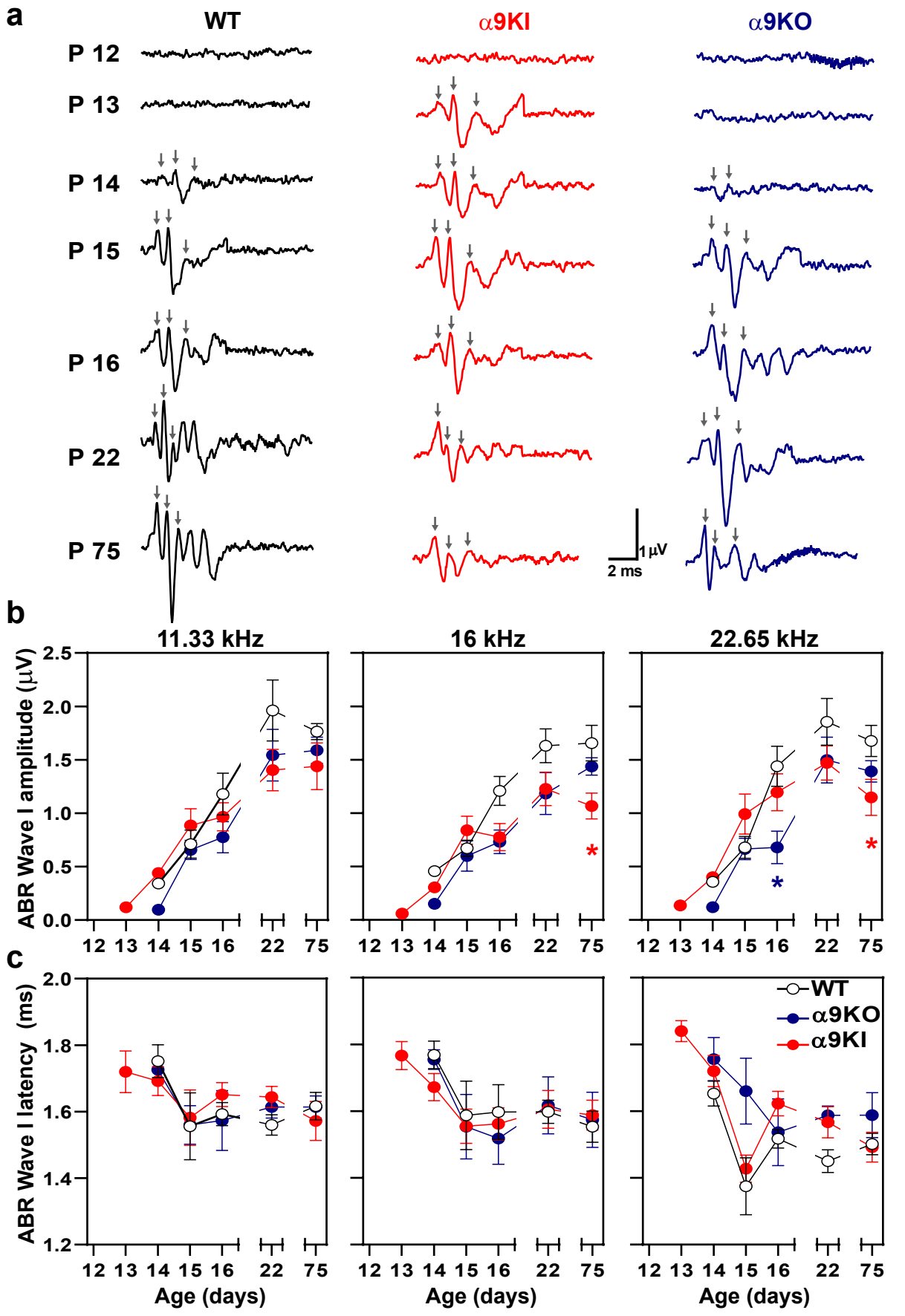
a
WT
α9KI
α9KO
P 12
P 13
P 14
P 15
P 16
P 22
P 75
1 μV
2 ms
b
11.33 kHz
16 kHz
22.65 kHz
ABR Wave I amplitude (μV)
2.5
2.0
1.5
1.0
0.5
0.0
12 13 14 15 16 22 75
c
ABR Wave I latency (ms)
2.0
1.8
1.6
1.4
1.2
WT
α9KO
α9KI
Age (days)

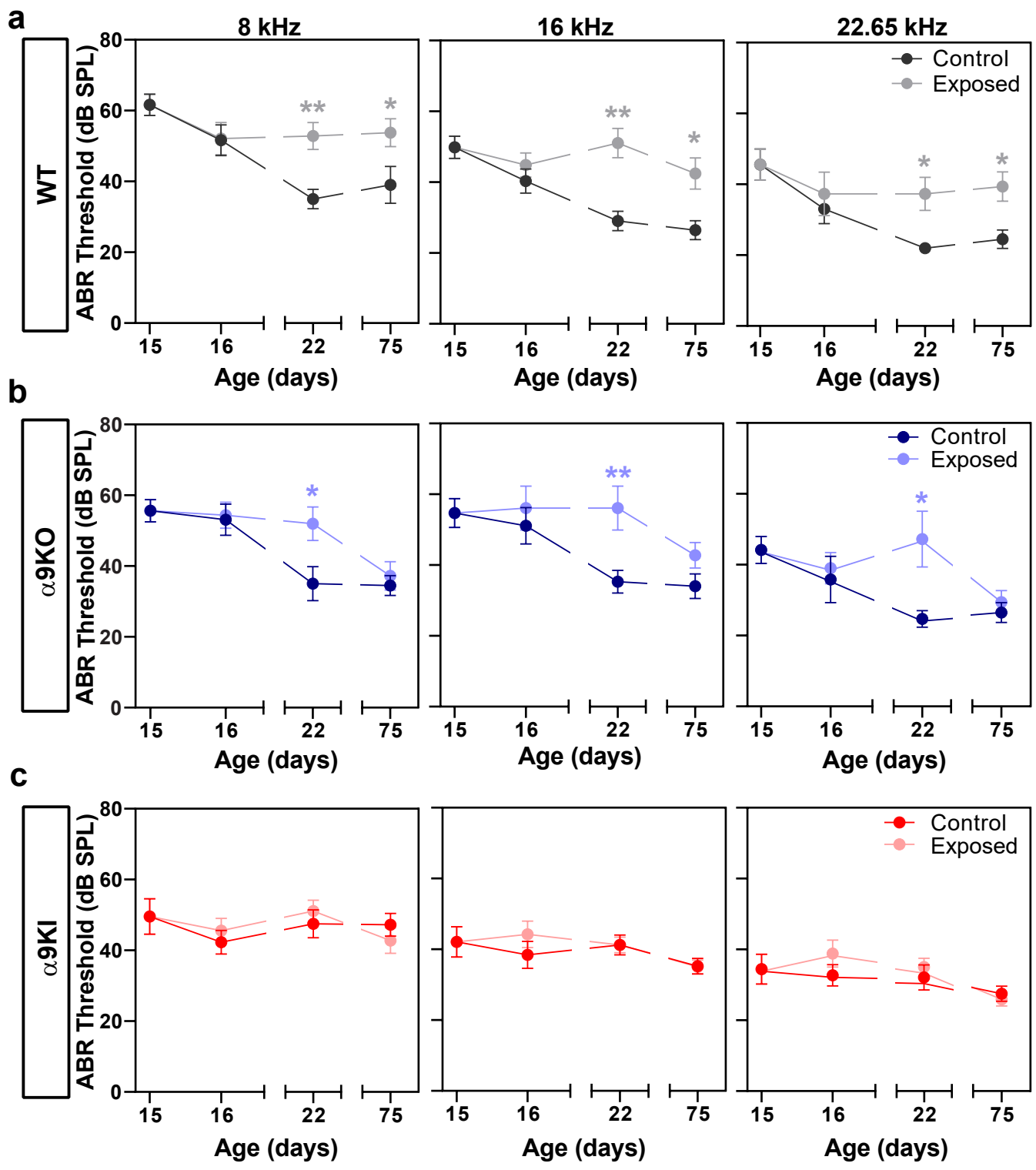
a
8 kHz
16 kHz
22.65 kHz
WT
ABR Threshold (dB SPL)
Control
Exposed
**
*
Age (days)
b
α9KO
c
α9KI
0
20
40
60
80
15
16
22
75

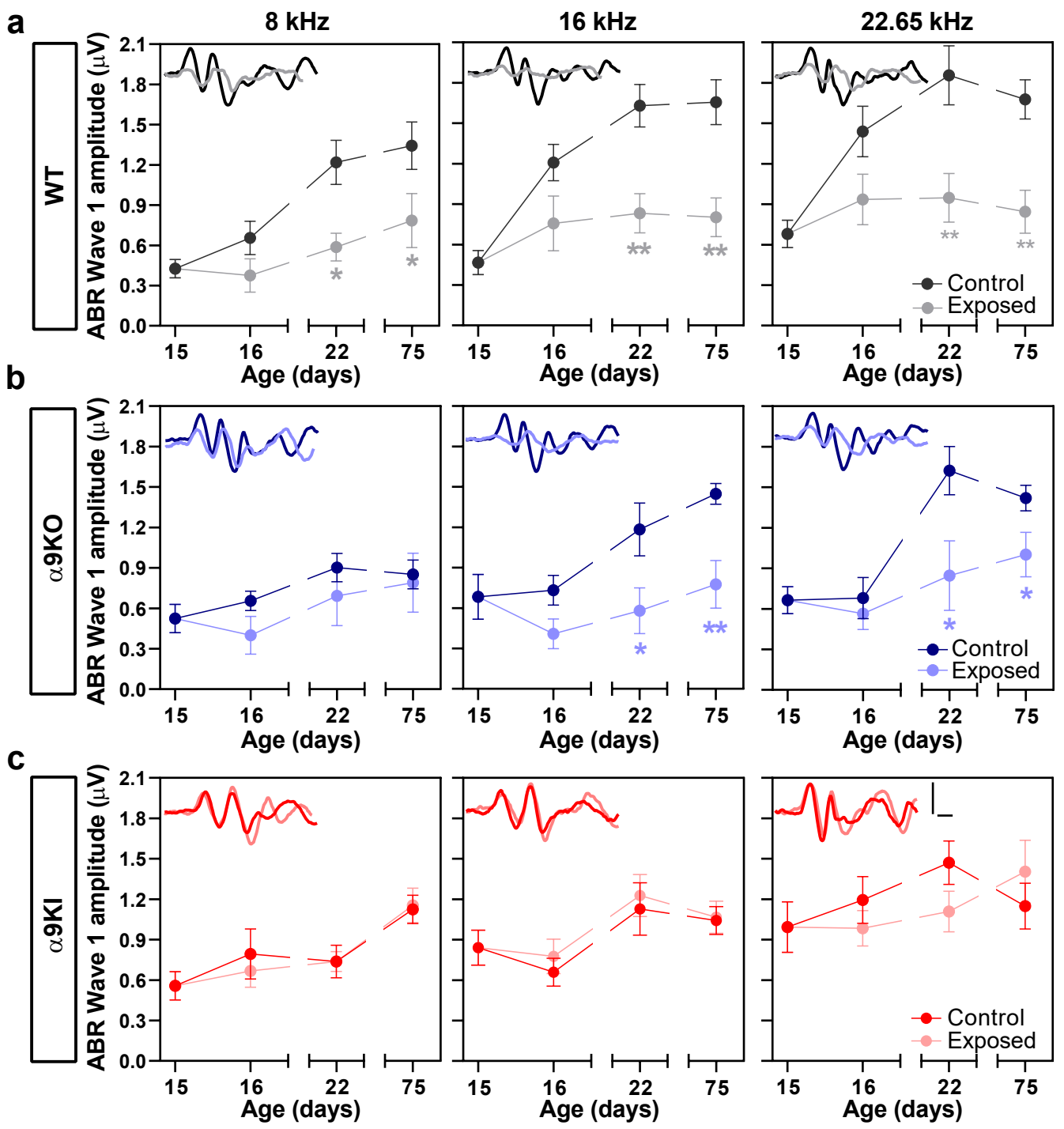
a
8 kHz
16 kHz
22.65 kHz
WT
ABR Wave 1 amplitude (μV)
2.1
1.8
1.5
1.2
0.9
0.6
0.3
0.0
15
16
22
75
Age (days)
*
**
Control
Exposed
b
α9KO
c
α9KI

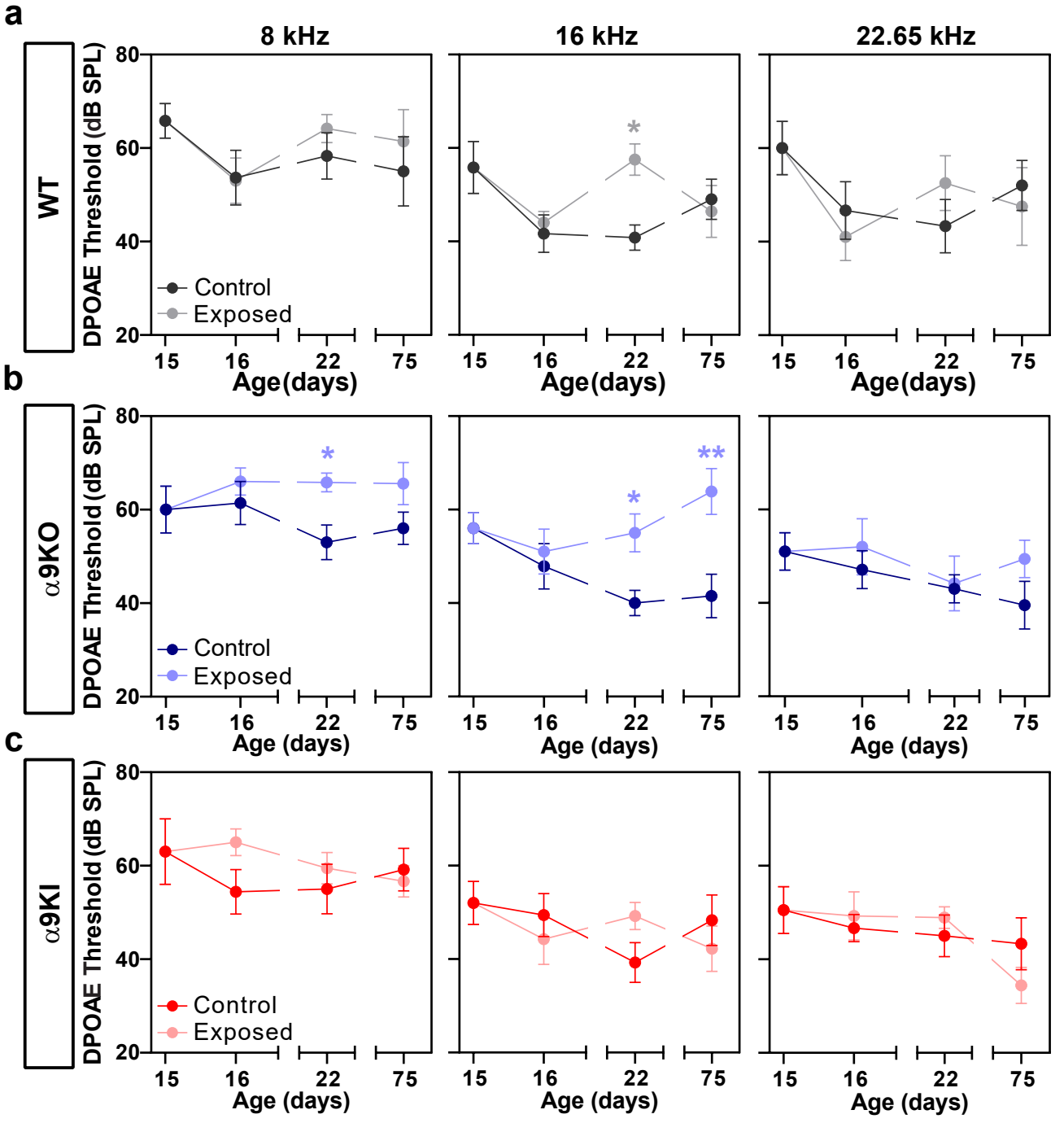
a
8 kHz
16 kHz
22.65 kHz
WT
DPOAE Threshold (dB SPL)
80
60
40
20
Control
Exposed
*
15
16
22
75
Age(days)
b
α9KO
Control
Exposed
*
*
**
Age (days)
c
α9KI
Control
Exposed
Age (days)

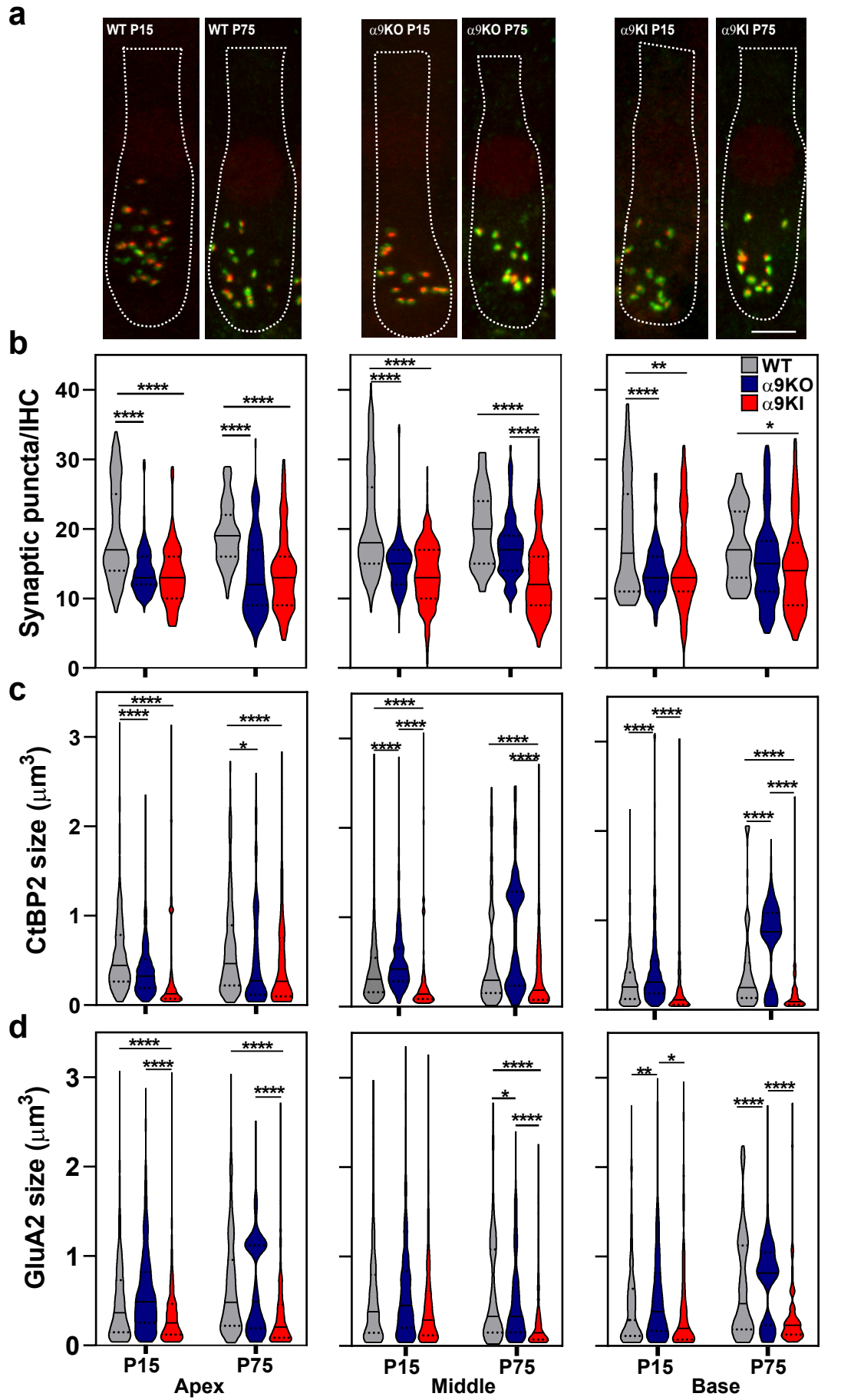
a
WT P15
WT P75
α9KO P15
α9KO P75
α9KI P15
α9KI P75
b
Synaptic puncta/IHC
WT
α9KO
α9KI
c
CtBP2 size (μm³)
d
GluA2 size (μm³)
P15
P75
Apex
Middle
Base

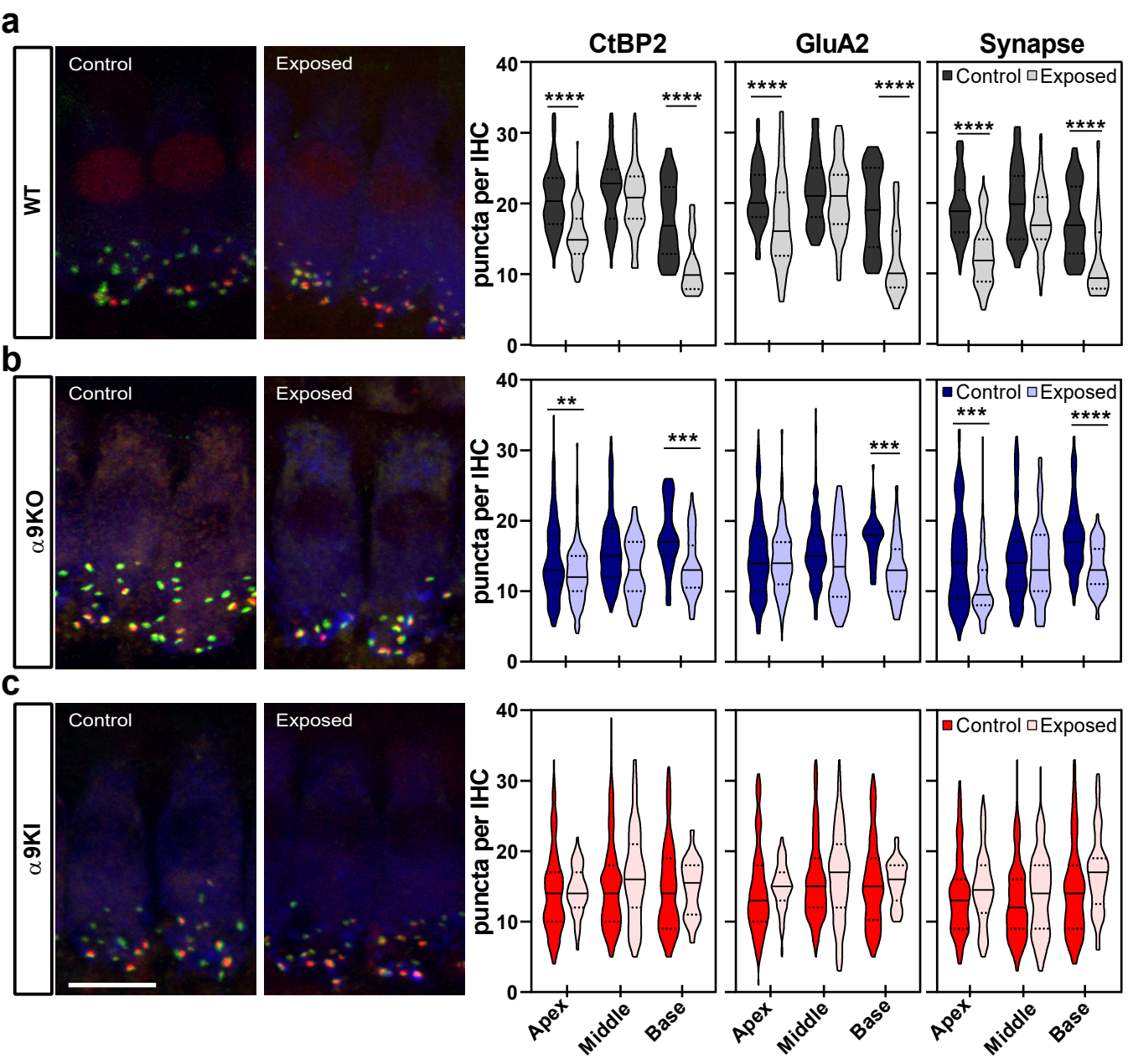
a
b
c
WT
α9KO
α9KI
Control
Exposed
CtBP2
GluA2
Synapse
puncta per IHC
0
10
20
30
40
****
**
***
Apex
Middle
Base

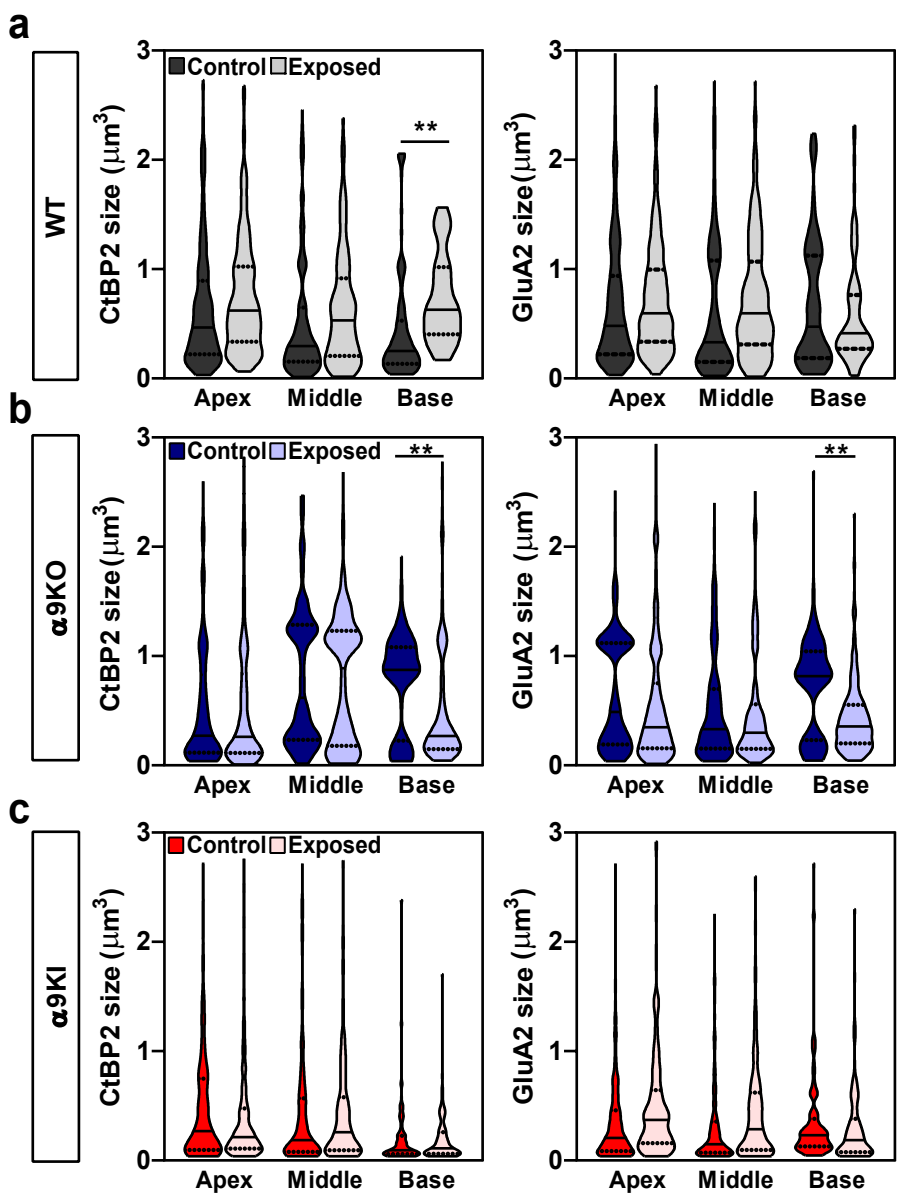
a
WT
Control
Exposed
CtBP2 size (μm3)
GluA2 size (μm3)
**
Apex
Middle
Base
b
α9KO
Control
Exposed
CtBP2 size (μm3)
GluA2 size (μm3)
**
**
Apex
Middle
Base
c
α9KI
Control
Exposed
CtBP2 size (μm3)
GluA2 size (μm3)
Apex
Middle
Base